Global Biogeochemical Cycles
Published 28 January 2021
https://doi.org/10.1029/2020GB006787

Anthropogenic Perturbations to the Atmospheric Molybdenum Cycle

Wong, Michelle Y.[1,2]†; Rathod, Sagar D.[3]; Marino, Roxanne[2]; Li, Longlei[4]; Howarth, Robert W.[2]; Alastuey, Andres[5]; Alaimo, Maria Grazia[6]; Barraza, Francisco[7]; Carneiro, Manuel Castro[8]; Chellam, Shankararaman[9]; Chen Yu-Cheng[10]; Cohen, David D.[11]; Connelly, David[12], Dongarra, Gaetano[6]; Gomez, Dario[13]; Hand, Jenny[14]; Harrison, R.M.[15,16]; Hopke, Philip K.[17,18]; Hueglin, Christoph[19]; Kuang, Yuan-wen[20]; Lambert, Fabrice[21,22]; Liang, James[17]; Losno, Remi[23]; Maenhaut, Willy[24]; Milando, Chad[25]; Monteiro, Maria Inês Couto[8]; Morera-Gómez, Yasser[26]; Querol, Xavier[5]; Rodríguez, Sergio[27,28,29]; Smichowski, Patricia[13,30]; Varrica, Daniela[6]; Xiao, Yi-hua[31], Xu, Yangjunjie[23]; Mahowald, Natalie M.[4,32]

[1]Cary Institute of Ecosystem Studies, Millbrook, NY, USA

[2]Department of Ecology and Evolutionary Biology, Cornell University, Ithaca, NY, USA

[3]Department of Atmospheric Science, Colorado State University, Fort Collins, CO, USA

[4]Department of Earth and Atmospheric Science, Cornell University, Ithaca, NY, USA

[5]Institute of Environmental Assessment and Water Research (IDEA-CSIC), Barcelona, Spain

[6]Dipartimento Scienze della Terra e del Mare, University of Palermo, Sicily, Italy

[7]School of Geography, University of Otago, New Zealand

[8]Coordenação de Análises Minerais, Centro de Tecnologia Mineral – CETEM, Rio de Janeiro, R.J., Brazil

[9]Department of Civil & Environmental Engineering, Texas A&M University, College Station, TX, USA

[10]National Institute of Environmental Health Sciences, National Health Research Institutes, Miaoli, Taiwan

[11]Australian Nuclear Science and Technology Organisation, Lucas Heights, New South Wales, Australia

[12]Department of Mathematics, Cornell University, Ithaca, NY, USA

[13]Comisión Nacional de Energía Atómica, Gerencia Química, San Martín, Buenos Aires, Argentina

[14]Cooperative Institute for Research in the Atmosphere, Colorado State University, Fort Collins, CO, USA

[15]School of Geography, Earth and Environmental Sciences, University of Birmingham, Edgbaston, Birmingham, United Kingdom

[16]Department of Environmental Sciences/Center of Excellence in Environmental Studies, King Abdulaziz University, Jeddah, Saudi Arabia

[17]Clarkson University, Potsdam, NY, USA

[18]Department of Public Health Sciences, University of Rochester School of Medicine and Dentistry, Rochester, NY, USA

[19]Swiss Federal Laboratories for Materials Science and Technology (EMPA), Dübendorf, Switzerland

[20]Key Laboratory of Vegetation Restoration and Management of Degraded Ecosystems, South China Botanical Garden, Chinese Academy of Sciences, Guangzhou, China

[21]Department of Physical Geography, Pontifical Catholic University of Chile, Santiago, Chile

[22]Center for Climate and Resilience Research, University of Chile, Santiago, Chile

[23]Université de Paris, Institut de Physique du Globe de Paris, Paris, France

[24]Department of Chemistry, Ghent University, Gent, Belgium

[25]School of Public Health, Boston University, Boston, MA, USA

[26]Centro de Estudios Ambientales de Cienfuegos (CEAC), Cienfuegos, Cuba

[27]Izaña Atmospheric Research Centre, AEMET, Santa Cruz de Tenerife, Spain

[28]Estación Experimental de Zonas Áridas, EEZA CSIC, Almería, Spain

[29]Instituto de Productos Naturales y Agrobiología, IPNA CSIC, Tenerife, Spain

[30]Consejo Nacional de Investigaciones Científicas y Técnicas (CONICET), Buenos Aires, Argentina

[31]Research Institute of Tropical Forestry, Chinese Academy of Forestry, Guangzhou, China

[32]Cornell Atkinson Center for Sustainability, Cornell University, Ithaca, NY, USA

†Corresponding author: Michelle Wong (wongm@caryinstitute.org)

Key Points:

- We compiled atmospheric molybdenum (Mo) concentration data and compared observations to a three-dimensional global atmospheric aerosol model
- Anthropogenic activity has likely doubled atmospheric Mo globally, but with regional variation
- Mo turnover time for the top meter of soil ranges between 1000 to 1,000,000 years, with the shortest times in dust source regions and industrialized areas

Abstract

Molybdenum (Mo) is a key cofactor in enzymes used for nitrogen (N) fixation and nitrate reduction, and the low availability of Mo can constrain N inputs, affecting ecosystem productivity. Natural atmospheric Mo aerosolization and deposition from sources such as desert dust, sea-salt spray, and volcanoes can affect ecosystem function across long timescales, but anthropogenic activities such as combustion, motor vehicles, and agricultural dust have accelerated the natural Mo cycle. Here we combined a synthesis of global atmospheric concentration observations and modeling to identify and estimate anthropogenic sources of atmospheric Mo. To project the impact of atmospheric Mo on terrestrial ecosystems, we synthesized soil Mo data and estimated the global distribution of soil Mo using two approaches to calculate turnover times. We estimated global emissions of atmospheric Mo in aerosols (<10 μm in diameter) to be 23 Gg Mo yr^{-1}, with 40 to 75% from anthropogenic sources. We approximated that for the top meter of soil, Mo turnover times range between 1,000 to 1,000,000 years. In some industrialized regions, anthropogenic inputs have enhanced Mo deposition 100-fold, lowering the soil Mo turnover time considerably. Our synthesis of global observational data, modeling, and a mass balance comparison with riverine Mo exports suggest that anthropogenic activity has greatly accelerated the Mo cycle, with potential to influence N-limited ecosystems.

Plain Language Summary

Molybdenum (Mo) is an essential trace element that is important for terrestrial and aquatic ecosystems, as it is required for biological nitrogen fixation and uptake. Molybdenum is carried in particles to the atmosphere from sources, such as desert dust, sea spray, and volcanoes,

resulting in losses and sources to different ecosystems. Atmospheric Mo deposition is essential on long time scales for soils which have lost Mo due to soil weathering, with consequences for nitrogen cycling. Anthropogenic changes to the Mo cycle from combustion, motor vehicles, and agricultural dust, are likely to be large, and have more than doubled sources of Mo to the atmosphere. Locally, anthropogenic changes to Mo in industrialized regions can represent a 100-fold increase in deposition, and may affect nitrogen cycling in nitrogen-limited ecosystems.

1 Introduction

Low bioavailability of molybdenum (Mo), an essential trace nutrient utilized as a cofactor in the nitrogenase enzyme that catalyzes biological nitrogen (N) fixation, can constrain N fixation in terrestrial (Dynarski & Houlton, 2018) and freshwater ecosystems (Glass et al., 2012). Nitrogen is a limiting nutrient across many ecosystems (e.g. LeBauer & Treseder, 2008; Vitousek & Howarth, 1991; Wang & Houlton, 2009), and in these ecosystems N fixation can enable higher productivity and carbon (C) uptake (Houlton et al., 2008; Thornton et al., 2009). Molybdenum limitation of N fixation has been found in some boreal, temperate, and tropical ecosystems (Perakis et al., 2017; Rousk et al., 2016; Silvester, 1989; Wurzburger et al., 2012), while not in other tropical ecosystems (Wong et al., 2020a). In freshwater systems, Mo availability can also constrain N fixation, nitrate uptake, and thus C assimilation in some lakes (Glass et al., 2012; Romero et al., 2013). Atmospheric deposition is a more important source of Mo than local bedrock weathering in some freshwater systems (Carling et al., 2017). In the absence of Mo, many N-fixing bacteria can synthesize “alternative” vanadium (V) and iron (Fe)-only nitrogenase isoforms (Darnajoux et al., 2019; McRose et al., 2017; Zhang et al., 2016). However, alternative nitrogenases show lower specific activity in laboratory experiments (Eady,

110 1996) and may be less efficient for N fixation, and it is unknown how widespread their activity is
111 in the environment. Natural atmospheric deposition of Mo may be an essential source of Mo for
112 ecosystems on long (>10,000 year) time scales (Wong et al., 2020b), similar to long-range
113 atmospheric inputs of phosphorus (P) to the Amazon (Yu et al., 2015), but anthropogenic activity
114 may be affecting the magnitude and distribution of Mo to the atmosphere.

115 Both global emission estimates and local observations suggest large anthropogenic
116 sources of atmospheric Mo (Bozlaker et al., 2013; Hueglin et al., 2005; Nriagu & Pacyna, 1988),
117 with previous syntheses estimating roughly equal contributions from anthropogenic and natural
118 sources (Nriagu 1989; Nriagu & Pacyna, 1988). Molybdenum is used in alloys, lubricants, and
119 catalysts, and can be a by-product of tungsten and copper mining (NPCS, 2009). Other
120 anthropogenic sources of Mo include petrochemical plants and fossil fuel combustion (Boonpeng
121 et al., 2017; Danadurai et al., 2011), mining facilities (Hernández-Pellón & Fernández-Olmo,
122 2019), and vehicles which release Mo through engine wear (Gonet & Maher, 2019), lubricating
123 oils (Alves et al., 2015), catalytic converters (Dillner et al., 2005; da Silva et al., 2008), and
124 braking on roads (Fujiwara et al., 2011; Hueglin et al., 2005).

125 Natural sources of atmospheric Mo, such as desert dust, sea-spray aerosols, volcanoes,
126 primary biogenic particles, and wildfires (Nriagu, 1989; Wong et al., 2020b), may have different
127 spatial distributions than anthropogenic sources, such as combustion, vehicle-related emissions,
128 and agricultural dust. In addition, the higher solubility of many elements from anthropogenic
129 aerosols due to their chemical and surface associations, reactions during the combustion
130 processes, higher carbon content, and smaller particle sizes (Desboeufs et al., 2005; Jang et al.,
131 2007; Sedwick et al., 2007; Voutsa & Samara, 2002) suggest that anthropogenic aerosols could
132 impact ecosystems more rapidly than natural aerosols such as desert dust. For example, 15-50%

of the total Mo in coal fly is water-soluble (Izquierdo & Querol, 2012; Moreno et al., 2005). Furthermore, atmospheric processing, such as interaction with sulfate plumes, can increase the solubility of Mo, and may be associated geographically more with anthropogenic sources compared to natural sources (Hsu et al., 2010; Meskhidze et al., 2005).

While the spatial distribution of natural atmospheric Mo deposition and its impact on long-term ecosystem function has been examined (Wong et al., 2020b), no previous studies have modeled anthropogenic Mo sources or compared current deposition estimates with observational data. Natural atmospheric Mo deposition has likely shaped ecosystem function across long timescales, but anthropogenic Mo may have begun to accelerate Mo cycling in the past few decades. We present for the first time a synthesis of the observational and modeling evidence for the anthropogenic perturbation in atmospheric Mo for $PM_{2.5}$ and PM_{10} (atmospheric particulate matter, PM, <2.5 and 10 μm in aerodynamic diameter, respectively), as well as their spatial distribution, and discuss the potential impact of anthropogenic Mo on terrestrial ecosystems. We focus on $PM_{2.5}$ and PM_{10} because they are commonly measured in the atmosphere as well as included in the model used here (Mahowald et al., 2014; Ryder et al., 2019).

2 Materials and Methods

2.1 Atmospheric observations

2.1.1 Description of atmospheric observations

To synthesize observational atmospheric Mo data, we collected data from multiple observational networks and sites that record particulate matter (PM) atmospheric concentrations, some of which include elemental and/or chemical speciation. Observations were taken using several different methods and span many years as described in each paper for each set of

observations (Figure 1, Supporting Information Data Set 1). From a compilation of these observations (Supporting Information Supplementary Methods), we can both infer the sources from a compositional analysis and by comparing observations against model predictions (Figure 1; Supporting Information Data Set 1). We compiled observations of aerosols in both the $PM_{2.5}$ and PM_{10} size categories (PM < 2.5μm and 10μm in aerodynamic diameter, respectively) (Mahowald et al., 2011) when available. The most common method for sample collection was by filter sampling, separating aerosols into $PM_{2.5}$ and PM_{10}. For Mo quantification, X-ray fluorescence was most commonly used. Further methods and descriptions for each site, along with other elemental data, total particulate matter, and chemical composition, are discussed within the respective studies (Figure 1, Supporting Information Data Set 1).

We focus on $PM_{2.5}$ and PM_{10} because they are commonly measured in the atmosphere as well as included in models because of the longer residence time of aerosols <10 μm in aerodynamic diameter than that of aerosols larger in size, although there is evidence that the larger particles can travel long distances as well (Mahowald et al., 2014; Ryder et al., 2019). Instead of measuring PM_{10} and $PM_{2.5}$, some stations measured coarse PM ($PM_{10\text{-}2.5}$, mass of particles with aerodynamic diameters between 2.5 and 10 μm) along with fine ($PM_{2.5}$). If both fine and coarse modes were measured at a site, they are summed and compared as if they were PM_{10} observations (Figure 1). Some observational networks or sites were unable to quantify Mo if concentrations were lower than their detection limits. We note that there are many sites, such as from the Interagency Monitoring of Protected Visual Environments (IMPROVE) remote/rural network in the U.S., which focus only on $PM_{2.5}$ (Hand et al., 2017, 2019), with less than 50% of the Mo values above the detection limit (Figure 1).

For PM_{10} and $PM_{2.5}$, samplers can differ in the sharpness of their size cutoff (Hand et al., 2019). For example, comparisons between collocated sites from the U.S. EPA and IMPROVE suggested that the coarse aerosol mass ($PM_{10-2.5}$) from the EPA sites were 10% higher than at IMPROVE sites, with a 28% difference between these estimates (Hand et al., 2019). The correlation coefficient was 0.9 with a slope of 0.9, suggesting overall a good agreement, although the different biases between samplers should be kept in mind while evaluating Mo atmospheric concentrations both in the PM_{10} and $PM_{2.5}$ size fractions (Hand et al., 2019).

While we focused on observational data for PM_{10} and smaller particles based on the size modes that our model simulates, we also collected bulk/total atmospheric (dry and wet) deposition data (all particle sizes) in the Supporting Information (Figure S5) to compare to our model simulations, as bulk/total atmospheric deposition also has an ecological impact as it includes all particles that can be distributed to the atmosphere. However, we note that these data are not directly analogous to the model, and that absolute dry and wet deposition rates are often difficult to measure robustly (Heimburger et al., 2012; Prospero et al., 1996).

2.1.2 Analysis of atmospheric observations

Annual means of atmospheric observations at each site are calculated for all values at each station that are above the detection limit and reported here. Because Mo concentrations are usually low in atmospheric aerosols (<1 ng m^{-3}), we considered whether we were biasing our results towards higher values because in some cases, a large proportion of the data were below the detection limit. If more than 50% of values at a site were reported as above the detection limit, we used one-third of the minimum detection limit for any samples below detection limit. However, if less than 50% of the data at a site were above the detection limit, we excluded the data in our annual values. Instead, we included the data to calculate an upper bound using their

respective detection limits. Here, we present both the average values (that include more than 50% of the values above the detection limit), as well as bounded values that include the upper bound of studies with more than 50% of samples under the detection limit (Supporting Information Data Set 1).

In order to compare the model to observational data, records from the observations from different sites were combined into a mean within a grid cell that was two times the model resolution, or 2° x 2°. This process averages the observations over a spatial scale appropriate for comparison with the model (Schutgens et al., 2016). We used the same procedure to count the number of observations in each grid cell (Figure 1).

We conducted an additional analysis at stations from a network in Switzerland (Hueglin et al., 2005) using compositional analysis (Qu et al., 2020). These sites were chosen because of the high spatial and temporal resolution and clear detection limits. We processed the atmospheric concentrations of different elements with the "compositions" package (van den Boogaart et al., 2014; R Core Team, 2018) which provides the "acomp" function, transforming concentrations prior to a principal component analysis to create a biplot (Supporting Information Figure S2). The outcome of this approach is a simple visual analysis of the similarities and differences between the elemental content in PM over time or space, displaying the relative variation more readily, allowing us to assess potential sources of Mo which may vary over space and time.

2.2 Atmospheric modeling

We simulated atmospheric Mo emission, transport, and deposition in a new Mo module developed based on the aerosol parameterizations within the Community Atmosphere Model, version 6 (CAM6), the atmospheric component of the Community Earth System Model (CESM) developed at the National Center for Atmospheric Research (NCAR) (Hurrell et al., 2013; Liu et

al., 2011; Scanza et al., 2015). Simulations were conducted for six years, with the last five years (2007-2011) used for the analysis (Computational and Information Systems Laboratory, 2019). The model simulates three-dimensional transport and wet and dry deposition for gases and aerosols based on MERRA2 winds (Gelaro et al., 2017). The model included prognostic dust, sea salts, black carbon, organic carbon and sulfate aerosols in the default version using a modal scheme (Liu et al., 2011). For this study, we added the ability to carry Mo. Between CAM5 and CAM6, the size bounds of the coarse mode were reduced in the default version to better simulate stratospheric aerosols from volcanic eruptions. For this study, the coarse mode size was returned to the CAM5 size to better simulate coarse mode aerosols. Note that we used a different model version (CAM6) than used in Wong et al. (2020b) (CAM4), and thus the magnitude of natural sources changed compared to that study.

Uncertainties in source strengths were large for both the natural sources (desert dust, sea-salt aerosols, volcanoes, primary biogenic particles, wildfires) and the anthropogenic sources (combustion, braking, agricultural dust). Therefore, we included a range of values (typically a factor of ten) for the global total based on the range in source Mo concentrations (Table 1). In some simulations, we also included a 'high' anthropogenic scenario to test if the model better explained the observational data (Table 1).

2.2.1 Desert dust

For Mo in desert dust, we assumed a constant fraction of Mo (1.1 mg Mo kg^{-1}) in dust reported by Wong et al. (2020b), well within the range of the crustal abundance of Mo at 1-2 mg Mo kg^{-1} (Rudnick & Gao, 2003; Taylor & McLennan, 1995) which is slightly lower than the 2-5 mg Mo kg^{-1} used in the review of Nriagu (1989) (Table 1). In the CAM model, mineral dust is entrained into the atmosphere in unvegetated dry, arid regions with easily erodible soils during

247 strong near-surface wind events (Zender et al., 2003). The Modal Aerosol Model (Liu et al.,
248 2011) includes three size modes corresponding to the Aitken, accumulation, and coarse modes.
249 We used the CAM5 mass median diameter and sigma as well as the edges of the coarse mode
250 instead of the CAM6 to better simulate the coarse mode and accumulation mode separately,
251 following Li et al. (2020). In each aerosol size mode, Mo was transported and deposited
252 separately using the size fractionation proposed by Albani et al. (2014). The default CAM6
253 model was modified to use the Kok dust emission scheme (Kok et al., 2014a; Kok et al., 2014b)
254 and tuned to a global mean global aerosol optical depth (AOD) of 0.030 (Li et al., 2020) as
255 suggested to better match observations (Ridley et al., 2016). The dust emission, transport and
256 deposition were all prognostic, varied with each time step, and included seasonality (Kok et al.,
257 2014b). We estimated Mo emissions from desert dust to be 6.8 Gg Mo yr^{-1}, but with a large
258 range of 3.2-32 Gg Mo yr^{-1} due to the large uncertainty in both the dust budgets and the
259 concentration of Mo in dust (Table 1).

260 **2.2.2 Agricultural dust**

261 Land-use dust from agricultural lands could also be a source of Mo, as the concentrations
262 of Mo in soils are likely enriched in agricultural lands from the addition of Mo and P fertilizer,
263 which also contains Mo (Barron et al., 2009; Charter et al., 1995). Agricultural production and
264 related changes to the hydrologic cycle have led to increased anthropogenic dust (e.g. Ginoux et
265 al., 2012). Here we used datasets of crop fraction of agricultural land for the present day, from
266 the Coupled Model Intercomparison Project Phase 5 (CMIP5) inventory, in order to identify the
267 relevant regions and multiply by the estimates of desert dust generated using the same algorithm
268 for natural lands described above (Hurtt et al., 2011). We approximated that land-use sources of
269 dust were 25% of the total dust as estimated from satellites (Ginoux et al., 2012), and used the
270 prognostic dust scheme for the source, transport and deposition of the agricultural dust as a
271 separate tracer. The Mo concentration in agricultural sources of dust was assumed to be higher
272 than in natural lands. We used 2 mg Mo kg^{-1} as the best estimate and 5 mg Mo kg^{-1} for the high
273 estimate (Table 1, Supporting Information Table S2). We estimated agricultural dust emissions
274 to be 2.8 Gg Mo yr^{-1}, with a high estimate of 7.1 Gg Mo yr^{-1}.

275 **2.2.3 Sea-spray aerosols**

276 Sea-spray aerosols are entrained in the atmosphere from the ocean surface under high
277 wind or wave conditions (O'Dowd & de Leeuw, 2007). We used the same approach as Wong et
278 al. (2020b) with CAM6. Briefly, we used a constant concentration of Mo in seawater and the
279 existing sea-spray aerosol module (Liu et al., 2011) and a value of 0.29 mg Mo kg^{-1} of sea-spray
280 aerosol (Table 1), assuming sea-spray aerosol Mo concentrations reflect that of seawater (Wong
281 et al., 2020b). Sea-spray aerosols are prognostic in the model, based on wind speeds, sea-ice, and
282 temperature relationships (Liu et al, 2011). Sea-spray aerosol emission estimates were 0.75 Gg

283 Mo yr^{-1} and were assumed to be uncertain here (range 0.38-3.8 Gg Mo yr^{-1}; Table 1) due to the
284 uncertainty in sea spray aerosol budgets (Mahowald et al., 2011).

285 **2.2.4 Volcanoes**

286 Volcanic aerosols can be important local sources from non-eruptive volcanoes (Wong et
287 al., 2020b). Eruptive volcanoes could also be important, however, no appropriate long-term
288 dataset is available, so we focused on non-eruptive emissions using the same approach as Wong
289 et al., (2020b) but with CAM6. Briefly, we used the Mo to sulfur (S) ratio to approximate
290 volcanic Mo emissions, normalized to estimates of S emissions from volcanoes from gridded
291 global data sets (Spiro et al., 1992) of non-erupting volcanoes, using a temporally constant rate.
292 We used a mass-based ratio of 4 x 10^{-4} of Mo/S from Nriagu (1989) (Table 1). Non-eruptive
293 volcanic emissions were estimated to be 0.71 Gg Mo yr^{-1} with a range of 0.35-3.5 Gg Mo yr^{-1}
294 (Table 1).

295 **2.2.5 Primary biogenic particles**

296 Primary biogenic particles, or airborne particles from biological material, such as
297 bacteria, spores, fungi, viruses, algae, and pollen, are not explicitly modeled in the default
298 CAM6, but can be important for trace elements in aerosols such as P (Mahowald et al., 2008).
299 Thus we included a simple temporally constant parameterization of primary biogenic particles
300 following Brahney et al. (2015) by assuming a leaf area index dependent source. We tuned the
301 global amount such that over the Amazon, primary biogenic particles represent ~50% of the
302 PM_{10} concentrations, as consistent with observations (Graham et al., 2003). Following Nriagu
303 (1989) we used a Mo emission factor of 1.0 mg Mo kg^{-1} of primary biogenic aerosols, slightly
304 higher than the upper bound of Mo concentration measurements made from vegetation, which
305 range from 0.02 to 0.45 mg Mo kg^{-1} (Table 1, Supporting Information; Data Set 4). This

emission factor gave us a global Mo source of 0.49 Gg Mo yr^{-1}, and we assumed a range of 0.25-2.5 Gg Mo yr^{-1} (Table 1).

2.2.6 Wildfires

Wildfires may also represent a source of Mo (Nriagu, 1989), and emission datasets based on satellite burned area or other proxies for black carbon (BC) are widely available (Van Marle et al., 2017; van der Werf et al., 2004). We used the Coupled Model Intercomparison Project wildfire dataset as an annually-averaged temporally constant source (CMIP6) (Van Marle et al., 2017). This dataset includes both natural and deforestation fires, as well as human suppression of current wildfires, and thus includes some impacts from human activities. To convert from BC to Mo, we used an emission factor of 0.5 mg Mo kg^{-1} burned mass (Nriagu, 1989), divided by the emission factor of BC of ~ 0.5 g kg^{-1} burned mass (Andreae & Merlet, 2001) to get a ratio of Mo/BC of 1000 mg kg^{-1} (Table 1). We estimated wildfire sources to be 0.02 Gg Mo yr^{-1} with a range of 0.01-0.1 Gg Mo yr^{-1}.

2.2.7 Anthropogenic combustion

To estimate anthropogenic emissions of Mo from combustion sources, we made a first estimate by using a Fe emission inventory and assumed co-occurrence of Mo with Fe, multiplying by an observed emissions ratio. In some studies, Mo was not detected (Machemer, 2004), and in others, the Mo/Fe ratio was as high as 0.1 (Ge et al., 2001) or as low as 0.0001 (Querol et al., 1995), indicating Mo occurrence and emissions from coal and smelting-related emissions can be highly variable. We multiplied a central and upper 'high' Mo/Fe ratio of 0.005 and 0.01 to the updated Fe inventory for 2010 in Speciated Pollutant Emissions Wizard (SPEW) (Bond et al., 2004; Rathod et al., 2020). The Fe emissions in SPEW include coal, smelting, fuel oil, and wood combustion in the industrial, transport, and residential sectors globally. The central

ratio is based on the averaged observed Mo/Fe ratio in coal combustion and smelting-related emissions in Meij, (1994; 0.0025), Machado et al., (2006; 0.002), and Sylvestre et al., (2017; 0.008). We did not include fugitive emissions from Mo mining. Combustion emissions were assumed to be temporally constant and were about 11 Gg Mo yr^{-1} for the year 2010, with 95% coming from smelting and coal combustion. This source was large but with a large uncertainty associated with the estimated 'high' value being twice the base value (Table 1).

2.2.8 Vehicle braking

Braking-related emissions are the dominant non-exhaust vehicle emissions, and can contribute up to 50% of PM_{10} and 12% of $PM_{2.5}$ emissions from vehicles (Bozlaker et al., 2014; Grigoratos & Martini, 2015; Harrison et al., 2012). Braking-related emissions come from brake pads and brake discs, whereby the latter can contribute up to 70% of the total braking-related emissions (Hulskotte et al., 2014). Brake discs are generally made up of 95% Fe, 2% silica (SiO_2), and about 0.2% Mo (Hulskotte et al., 2014), the rest being copper (Cu), aluminum (Al), and Zn. The Mo fraction in brake dust PM ranges between 5-740 mg Mo kg^{-1} (Thorpe & Harrison, 2008; Grigoratos & Martini, 2014). The size distribution of braking-related emissions are generally unimodal with mass median aerodynamic diameters between 1 to 4 μm (Grigoratos & Martini, 2014), with sizes generally dominated by diameters of about 0.3 to 2 μm. We multiplied $PM_{2.5}$ and $PM_{10\text{-}2.5}$ vehicular combustion-related PM emissions (in SPEW) by 0.5 to estimate total PM emissions by brake-wear. Then, we multiplied the 2010 break-wear emissions by a central estimate of 500 mg Mo kg^{-1} brake-wear PM and assumed the 'high' anthropogenic upper bound to be about ten times the central emissions based on the uncertainty (1.8 to 8 mg PM km^{-1} $vehicle^{-1}$) in brake-wear emission factors in Grigoratos & Martini (2014) and the Mo fraction in brake-wear PM. These emissions ranged between 0.47 to 4.7 Gg Mo yr^{-1} for the year

2010 (Table 1). While vehicles in general may emit Mo through other pathways (Das & Chellam, 2020), we did not include other vehicle emissions here.

2.3. Soil Mo observations and estimates

To estimate the relative importance of Mo deposition on soil turnover time, we constructed a best estimate map of soil Mo concentrations. Current estimates assume a crustal abundance of 1-2 mg Mo kg^{-1} (Rudnick & Gao, 2003; Taylor & McLennan, 1995). Using the Thomson Web of Science Core Collection on 10 October 2019, we searched for the keywords "molybdenum" and "soil" and found 137 studies that reported a Mo concentration in surface soils based on a total or near-total digestion (Supporting Information; Data Set 3). If latitude and longitude were not reported, we identified the nearest coordinates based on the reported study location.

We used two methods to construct a Mo soil map. In the first method, we categorized available Mo data by soil type classification and extrapolated Mo concentrations by soil type using an approach similar to Scanza et al., (2015). Of the 137 studies, 68 provided soil classification information either in the United States Department of Agriculture (USDA) or the Food and Agriculture (FAO) taxonomic system, which we converted to the USDA classification. We assigned a median amount of Mo for each soil type then aggregated up to the 1°x1° USDA-NRCS Global Soil Regions map based on a reclassification of the FAO-UNESCO Soil Map of the World (Batjes, 1997), and data on Mo within different USDA's soil taxonomy orders as compiled here (Supporting Information Table S1; Data Set 3). The within soil order variability of Mo concentrations is similar to the between order soil variability (Table S1), so the estimated spatial distribution of Mo in soils using this method does not compare well against observations (Supporting Information Figure S1a). For some soil orders, only three studies per soil order were

reported, leaving the method of extrapolation by soil order as highly uncertain. In the second method, we extrapolated Mo concentrations in soils geographically through kriging interpolation using longitude and latitude coordinates. Because this method is simply an extrapolation of the available data, it does compare well, by definition with available data (Supporting Information Figure S1c and d). Because of the limited data, we used both methods to estimate the Mo concentration in soils.

The turnover time of Mo in the soils due to atmospheric deposition, in years, was calculated as the ratio of the soil Mo estimated to 1 m depth in each grid cell divided by the deposition flux, as estimated in Section 2.2. Because soil Mo cannot be assumed to be in steady state, we estimate a "pseudo-turnover time," which allows us to examine the ecological relevance of atmospheric Mo to the soil Mo reservoir in units of years (Okin et al., 2004).

3 Results

We present several types of evidence of anthropogenic sources of Mo, starting with local gradients between urban and rural regions, and including references to compositional analysis of aerosol observations. We then show the spatial distributions of the *in-situ* concentration observations, compared to modeling with and without anthropogenic sources. Finally, we show the resulting deposition maps and calculate the turnover times in soils.

3.1 Analysis of specific sites

First, to better understand the nature of the sources of atmospheric Mo, we considered a few datasets where data are collected from cities and in nearby rural areas. Data collected from the sites in Switzerland, where a substantial fraction of the concentrations were above the detection limit for Mo, suggested that there was a clear gradient in the spatial distribution of Mo

398 with higher concentrations in the more urban areas (Figure 2a), along with higher PM in general
399 (Gianini et al., 2012a; Gianini et al., 2012b; Hueglin et al., 2005).
400 Second, compositional analysis on the observations across all sites in Switzerland
401 (Hueglin et al., 2005) using the approach by Qu et al. (2020) indicated that Mo is typically found
402 in urban aerosols (Supporting Information Figure S2). This approach removed the concentration
403 of aerosols and focused on the first two principal components of the composition using a selected
404 set of elements. The compositional results strongly suggest anthropogenic sources of Mo for both
405 $PM_{2.5}$ and PM_{10}; Mo concentrations tended to be higher in urban PM and that the PM with higher
406 Mo concentrations was also enriched in other typically urban aerosols components for both
407 $PM_{2.5}$ and PM_{10}.
408 Similarly, we examined compositional differences between two sites in Cuba where
409 samples were collected simultaneously at a rural and an urban site (Morera-Gómez et al., 2018).
410 Despite both sites being located on the coast with high deposition from sea-spray aerosols and
411 under the North African dust plume in a region with some of the largest atmospheric Mo
412 deposition rates (Wong et al., 2020b), the urban area was characterized by a higher Mo
413 concentration than the other site. The urban area also had a higher mixing ratio of Mo in PM
414 (concentration of Mo divided by the total mass of PM), suggesting a large anthropogenic
415 influence (Figure 2b). This high Mo/PM ratio was presumably due to the large petrochemical
416 industries in this region, including a cement plant fueled by petroleum-coke, an asphalt plant, a
417 power plant fueled by heavy crude oil, and Cuba's largest oil refinery. Bottom ash from the latter
418 two industries had high contents of Mo (720 and 114 mg Mo kg^{-1}, respectively; Alonso-
419 Hernández et al., 2011). Detailed source apportionment studies suggested that much of the
420 particulate Mo in this region was associated with road traffic (48%), combustion sources (22%),

with some contribution from marine aerosols (16%) and either cement industry or dust (10%) (Morera-Gómez et al., 2018). The more substantial proportion of road traffic Mo can be attributed to older cars running on diesel, which often concentrates heavy metals (Morera-Gómez et al., 2020). We also found similar results across three sites in Spain (Hernández-Pellón & Fernández-Olmo, 2019), where bulk Mo deposition rates were also higher closer to a manganese alloy plant than in urban background sites.

Finally, a long-term (26 year) observational dataset at one site in Northern Europe demonstrated that atmospheric Mo peaked in the 1990s (Supporting Information Figure S3 using data, from Laing et al. (2014a, 2014b). This anomalous peak was likely caused by an anthropogenic source of Mo, because neither an increase over time, black carbon concentration ($r=0.03$; Figure S3), nor non-sea-salt sulfate (Laing et al., 2013) can explain the peak.

3.2 Spatial distribution of atmospheric Mo

Our synthesis of the available observations of Mo in PM_{10} demonstrated that there were elevated concentrations observed across industrialized regions, such as Europe and Asia (Figure 3a). When we compared the model simulations with observations, we found that simulations with anthropogenic sources (Figure 3) were better at explaining Mo observations than only simulating with natural sources (Figure 4). When only natural sources were included, concentrations of Mo in industrialized regions, especially in Europe, were underestimated by several orders of magnitude (Figure 3 versus Figure 4). In some regions, the simulated anthropogenic estimate of emissions using our 'high' estimate was a better match to the available data, although in others the 'high' case overestimated the concentrations (Figure 3c). Although these results are difficult to verify with the limited observational data, the model simulations suggest that there is substantially more Mo in the atmosphere in Europe and Asia than in North

America, primarily because of the higher estimates of combustion sources in these regions. While the model simulations did not correlate statistically significantly with the observations, they agreed on the same order of magnitude of Mo in the atmosphere.

Because the Mo concentration is typically low in atmospheric aerosols, we could have potentially biased our results by only including reported data where Mo was above the detection limit. To minimize bias, as discussed in the Methods section, if the reported values were below the detection limit, we approached the issue in two ways: first, if more than 50% of the observations at a particular site were above the detection limit, we included one-third of the minimum detection limit in the annual average. Second, the sites with less than 50% of observations above the detection limit provided information in that the limit of detection represented an upper bound on the Mo value, which we included as an upper bound in a secondary analysis (Figure 3d). However, including the upper bound did not appreciably change our picture of the Mo in the atmosphere (Figure 3d vs. 3c).

While a majority of modeled Mo was estimated to be in the PM_{10} fraction due to the large desert dust, agricultural dust, and combustion sources, of which are 50-99% in the coarse fraction (Table 1), we also considered the distribution of Mo in the fine ($PM_{2.5}$) aerosol fraction. Similar to the PM_{10} Mo fraction, observations of fine aerosol Mo also showed the highest values across industrialized regions (Figure 5a) and the simulations with only the natural sources were much lower than the observations (Figure S4). Similar to PM_{10}, assuming that the anthropogenic emissions are on the 'high' end, the model matched the observations well in some places, such as some sites in Europe, Asia, and the North Pacific, while the model over-predicted in other sites (Figure 5b vs 5c). We also compared the modeled concentrations of $PM_{2.5}$ to the upper bound in the concentrations where we included stations for which more than 50% of the data were below

467 the detection limit (Figure 5d). There were many more sites that measured but did not detect Mo
468 in the $PM_{2.5}$ fraction, especially in the U.S., so the scatter plot shows many more measurements
469 than the $PM_{2.5}$ observations of detected Mo (Figure 5d vs 5b). These comparisons showed that
470 the modeled Mo was below the upper bound in most locations (Figure 5d).

471 When we compared total/bulk deposition observations to our model results (Supporting
472 Information Figure S5), we also found strong evidence of anthropogenic Mo sources, as our
473 model still underestimated deposition observations at half the sites (Supporting Information
474 Figure S5). Another error source likely arises from missing Mo-source aerosols with an
475 aerodynamic diameter greater than the cutoff size of 10 μm by the model. In addition, models
476 begin to underestimate dust aerosols compared to observations at a diameter greater than
477 approximately 5 μm (Adebiyi & Kok, 2020; Kok et al., 2017; Mahowald et al., 2014). This
478 failure to capture large particles, which may dominate the deposition close to the source areas,
479 and their transport by the model may also explain the model-observation discrepancy.

480 **3.3 Sources of atmospheric Mo**

481 Modeled Mo deposition rates ranged over three orders of magnitude, from 1 $\mu g\ m^{-2}\ yr^{-1}$ to
482 5000 $\mu g\ m^{-2}\ yr^{-1}$. From our spatially explicit model, we estimated that 8.77 Gg Mo yr^{-1} was
483 emitted from natural sources with a range of 4.4 to 44 Gg Mo yr^{-1}, while 14.3 Gg Mo yr^{-1} was
484 emitted from anthropogenic sources with a range of 14-34 Gg Mo yr^{-1} (Table 1). These results
485 suggest that between 40% to 75% (best estimate: 62%) of the atmospheric Mo sources were
486 anthropogenic. There are large uncertainties in natural sources of aerosols such as sea spray and
487 dust, where estimates (dust: 6.6 Gg Mo yr^{-1}; sea-salt aerosols: 0.75 Gg Mo yr^{-1}; volcanic
488 aerosols: 0.71 Gg Mo yr^{-1}) are different than those from Wong et al., (2020b) (dust: 4.3 Gg Mo

489 yr^{-1}; sea-salt aerosols: 1.6 Gg Mo yr^{-1}; volcanic aerosols: 0.22 Gg Mo yr^{-1}) due to the difference
490 in the models used. These model discrepancies are consistent with the large uncertainties in the
491 amount and composition of natural aerosols in general (e.g. Mahowald et al., 2011). In the case
492 of Fe, the differences between the modeled and observed aerosol concentrations were higher in
493 areas where the natural aerosols are the dominant source (Rathod et al., 2020).

494 The estimated distribution of deposition for both the current best estimate (Figure 6a) and
495 natural sources (Figure 6b) shows that while desert dust regions are the strongest natural sources
496 and have the largest deposition rates, there is also intense deposition in industrialized regions.
497 The ratio of current anthropogenic to natural sources of Mo in the model suggests that there is a
498 large perturbation (up to 100x higher) on Mo deposition rates in many regions in both the best
499 estimate and the 'high' anthropogenic case (Figure 6c and 6d). When we examine the relative
500 contribution of sources to total Mo deposition across regions (Figure 7), we found that desert
501 dust deposition dominated close to the main dust source areas and sea-spray aerosols over the
502 oceans (Wong et al., 2020b), anthropogenic combustion sources dominated in industrialized
503 regions, and agricultural dust dominated in cultivated areas (Figure 7, Table 1).

504 Natural sources of Mo from terrestrial regions, such as primary biogenic particles and
505 wildfires, can remove Mo from ecosystems (Kauffman et al., 1995; Mahowald et al., 2005). For
506 example, we estimated that in the Amazon (290°E to 320°E, 15°S to 0°N) wildfire aerosols
507 deposit 0.18 Gg Mo yr^{-1} and cause the release of 0.20 Gg Mo yr^{-1}, while primary biogenic
508 particles deposit 0.048 Gg Mo yr^{-1} and release 0.052 Gg Mo yr^{-1}. Thus, although most Mo is
509 locally 'recycled' within ecosystems, we estimate that within this grid cell, about 10% of Mo
510 from wildfires and primary biogenic particles escapes into the ocean each year, which over
511 geological time could result in a deficit. However, Mo in this grid cell is estimated to be replaced

512 by long-range transported sea-spray aerosol Mo (0.003 Gg Mo yr^{-1}) and desert dust Mo (0.01 Gg
513 Mo yr^{-1}), and has been enhanced by anthropogenic sources of Mo, especially combustion (0.08
514 Gg Mo yr^{-1}).

515 **3.4 Implications for changes in soil Mo turnover times**

516 To assess the relative impact of aerosol deposition on soil Mo, we estimated turnover
517 times across the top 1 m of soil, which reflects the importance of aerosol Mo inputs relative to
518 the modern soil Mo reservoir (Okin et al., 2004). Using two approaches of approximating Mo
519 soil concentrations (see Methods 2.3), we found that soil Mo turnover times vary between 1000
520 years at the shortest (in regions where desert dust is the dominant source for Mo) up to millions
521 of years (Figure 8). Anthropogenic sources shorten turnover times (0.01x) regardless of the
522 interpolation method for soil Mo because of the strong increase in Mo in industrialized regions.
523 These results suggest that Mo deposition from anthropogenic sources could perturb and
524 accelerate Mo turnover in some regions if anthropogenic activity continues at the same rate into
525 the future. However, these turnover times are still long (1000 years or more) compared to other
526 perturbations, such as deforestation or biomass burning (Andela et al., 2017; Hansen et al.,
527 2013), which have accelerated turnover times for P in biomass from 64 to 50 years in regions of
528 the Amazon (Mahowald et al., 2005).
529

530 **4 Discussion**

531 Our models and synthesis of observations suggest that anthropogenic activity has
532 substantially altered the atmospheric Mo cycle and are accelerating Mo turnover rates in soils.
533 From modeling emissions of Mo, we estimated that anthropogenic sources, 14 [14-34] Gg Mo
534 yr^{-1} (range in brackets), are likely to be equal to or exceed the natural sources, which we

estimated to be 8.8 [4.4-44] Gg Mo yr^{-1} (Table 1). Even when we included anthropogenic sources in our model, observations of Mo sometimes exceeded modeled estimates, suggesting that the model simulations may be underpredicting deposition in some regions. In areas with strong influence from industrialization, fires, and agricultural land-use change, these activities have likely altered Mo cycles by a factor of two or more (Figure 7). Anthropogenic perturbation of the Mo cycle is on the same order of magnitude as the alteration of other metals such Al, V, mercury (Hg), and lead (Pb) (Rauch & Pacyna, 2009; Schlesinger et al., 2017; Selin, 2009; Sen & Peucker-Ehrenbrink, 2012).

4.1 Sources of discrepancy between the model and observational data

Differences between the model and the observations could be due to our model only predicting source emissions, but not resuspension of particles that are captured by observations. For example, direct emissions from vehicle braking were included in the model, but atmospheric sources such as road dust resuspension, which can comprise up to 50% of PM_{10} and a quarter of $PM_{2.5}$ (Bozlaker et al., 2014), were not included. Thus resuspension of sources to the atmosphere may have contributed to the model underestimation in some regions with higher densities of industrialization.

In addition to resuspension of particles, model underprediction in some regions could also be from unaccounted sources that were not included in the model, such as fugitive mining, PM emitted from vehicle exhaust, and other non-exhaust sources of vehicle Mo. Direct vehicle exhaust sources include engine wear (Gonet & Maher, 2019) and catalytic converters (Dillner et al., 2005). Detailed analysis of sites in the region of Rio de Janeiro demonstrated that the largest source of Mo in PM_{10} came from catalytic converters (da Silva et al., 2008) due to the rising usage of Pd-Mo/Al_2O_3 catalysts in Brazil (De Mello et al., 2003; Schmal et al., 1999), which we

were unable to include in our model. While we considered vehicle braking emissions based on correlations with Fe, we did not account for other non-exhaust related emissions, such as lubricants, where Mo sulfides are often added (Amato et al., 2010) and can compose between 5-29% of brake lining (Thorpe & Harrison, 2008).

4.2 Mass balance of Mo deposition with riverine exports

Comparing annual Mo riverine export to total deposition estimates from our model also suggests anthropogenic perturbation of the Mo cycle. From our synthesis of Mo in riverine samples (Supporting Information; Data Set 5), we estimated that around 21 Gg Mo yr^{-1} moved from terrestrial ecosystems through rivers to oceans every year, based on a median Mo river concentration of 0.56 μg Mo L^{-1} (Supporting Information; Data Set 5) and an annual discharge of 37,288 km^3 yr^{-1} (Dai & Trenberth, 2002). The riverine estimate of 21 Gg yr^{-1} fell close to our median atmospheric deposition estimate of 23 Gg Mo yr^{-1} (Table 1). However, the riverine export fluxes typically only represent export from terrestrial ecosystems, while our deposition estimates represent global fluxes to land and oceans. Thus, the large riverine estimates relative to our modeled estimates also suggest significant anthropogenic inputs. Our riverine Mo also exceeds the previous estimate of 17.3 Gg Mo yr^{-1} from the late 1970s (Martin & Meybeck, 1979) but falls below the recent estimate of 36 Gg Mo yr^{-1} (Sen & Peucker-Ehrenbrink, 2012), which implies that our riverine estimates of Mo are relatively conservative.

4.3 Impacts of anthropogenic Mo deposition on N cycling

Human perturbation of the Mo cycle is likely relieving Mo limitation on N fixation in regions isolated from strong N deposition. First, anthropogenic sources of Mo likely have stronger effects on N cycling relative to natural sources, as anthropogenic sources are typically more soluble (Desboeufs et al., 2005). Second, Mo as a constraint on N fixation is seemingly

widespread across many terrestrial ecosystems (Dynarski & Houlton, 2018), and in N-limited areas, increased Mo deposition may facilitate higher rates of N fixation. As discussed by Wong et al. (2020b), experimental addition rates of 39 μg Mo m^{-2} yr^{-1} have been found to stimulate free-living N fixation on a tropical forest floor (Barron et al., 2009), well within the estimated annual rates of current total Mo deposition (8 to 80 μg Mo m^{-2} yr^{-1} across many ecosystems (Figure 6). While Mo was added in a soluble, bioavailable form in the experiments of Barron et al., (2009), we present these rates as an example for the scale at which increases in Mo availability can impact N fixation, particularly over decades as deposition accumulates in the ecosystem. Third, in areas with Mo limitation, such as regions that are isolated from low external inputs of Mo with leaf litter concentrations less than 200-300 ng Mo g^{-1} leaf litter (Darnajoux et al., 2019; Reed et al., 2013), that are isolated from low external inputs of Mo, alternative nitrogenases may play an important role (Darnajoux et al., 2017; Zhang et al., 2016). Genes encoding alternative nitrogenases have been found in a variety of terrestrial ecosystems (Betancourt et al., 2008). Anthropogenic perturbation of the Mo cycle may shift alternative nitrogenase activity towards the more common and preferred Mo-based form of nitrogenase (Eady, 1996). Darnajoux et al. (2019) sampled across a gradient of atmospheric metal deposition in a northeastern American boreal forest and found an inverse correlation between high Mo deposition, indicated by Mo contents in lichens, and alternative vanadium-based nitrogenase activity. These results suggest that increased anthropogenic Mo deposition in previously pristine ecosystems that received little to no natural Mo or N deposition may enhance N fixation.

Terrestrial regions where Mo limitation have been found, which include several temperate, tropical, and boreal ecosystems (Dynarski & Houlton, 2018; Wong et al., 2020b; and references therein), may be particularly sensitive to anthropogenic Mo inputs. Other regions that

may be similarly sensitive to anthropogenic perturbations of the Mo cycle are regions where N limitation is strong and new inputs of Mo from weathering or natural atmospheric deposition are low. These areas include North American boreal forests, which may be affected by tar sands (Robertson et al., 2019), recovering Neotropical tropical forests (Batterman et al., 2013; Davidson et al., 2007) and savannas, which may be affected by biomass burning and agricultural dust, and recovering Asian tropical forests, which may be affected by combustion.

As temperatures and CO_2 concentrations increase and precipitation patterns change, the demand for N and thus increased N fixation may increase and exacerbate Mo limitation (Hungate et al., 2004; Zheng et al., 2020) in regions isolated from increasing N deposition inputs. While Mo limitation has been found across a few ecosystems, these studies have been concentrated in certain regions (Dynarski & Houlton, 2018). Before we can fully understand or predict how anthropogenic Mo may be affecting the N cycle, future research should focus on where and when Mo is limiting and contextualize Mo limitation with C, N, and P availability (Wong et al., 2020a; Wurzburger et al., 2012; Zheng et al., 2018).

Ultimately, the influence that anthropogenic Mo inputs will have on ecosystem function depends on the stoichiometry of other elemental inputs, such as N and P, and the nutrient status of the ecosystem being impacted (Figure 9). The signature of N deposition across the global is large, and anthropogenic N inputs will likely continue to increase in the future (Peñuelas et al., 2012, 2013). In these regions where anthropogenic N deposition inputs are large, stimulation of N fixation from increased atmospheric Mo may be offset (Bauters et al., 2018; Dentener et al., 2006). When examining Mo deposition together with N and P deposition, the largest sources of anthropogenic Mo tend to co-occur with the highest rates of N deposition, and the largest sources of natural Mo co-occur with the largest sources of atmospheric P (Figure 9 a and b). Regions that

receive low rates of N deposition and high rates of P deposition (or a lower N:P ratio) will likely be more sensitive to Mo as relieving P limitation would shift the ecosystem towards N limitation where increased Mo is advantageous. Other regions where Mo deposition may impact ecosystem function are regions where anthropogenic activity has accelerated Mo cycling to a greater extent than N and P cycling alone in many terrestrial ecosystems, as evidenced by the decrease in current to preindustrial N:Mo and P:Mo ratios in many temperate, boreal, and tropical regions (Figure 9c and d).

The large increase in atmospheric Mo will likely increase the imbalance between N and P globally, as anthropogenic N inputs have greatly exceeded P inputs (Peñuelas et al., 2012, 2013). In addition to the role of Mo in N fixation, Mo is essential for dissimilatory nitrate reduction, reducing nitrate to nitrite, often a rate-limiting step in N assimilation (Begara-Morales et al., 2020). Relieving any Mo constraints on the N cycle will contribute to increasing P limitation in both natural and agricultural ecosystems, which could impact ecosystems ranging from changing stoichiometry, species composition, and genomic composition (Peñuelas et al., 2012). The increased imbalance between the N and P cycles, and therefore ecological impact, may be greatest in the Northern Hemisphere, where both current to preindustrial N and Mo deposition are the highest (Figure 9e).

4.4 Limitations of the observational data and model

This paper represents a first attempt to constrain the spatial distribution of anthropogenic sources such as from combustion, braking, and land use. Most of the observations presented here were located in industrialized countries. To better understand the atmospheric contribution to the Mo cycle, more observations of concentrations and deposition are required. In addition, we also need a better understanding of the sources of Mo. For example, we used a recent Fe emission

compilation as a baseline for Mo from combustion, as most Mo co-occurs with Fe), however more in-depth consideration of Mo and other ecologically important metals, especially from mining and smelting (Rathod et al., 2020) would improve estimates. Finally, constraining emission factors from natural sources as well as from vehicle emission processes will improve our estimates of modeled Mo in remote as well as industrial and urban areas (Das & Chellam, 2020).

5 Conclusions

Low Mo availability can constrain N fixation and uptake in some terrestrial and aquatic ecosystems. Atmospheric deposition of Mo is likely an important source of Mo in N-limited terrestrial ecosystems with highly weathered soils, and previous studies have suggested substantial anthropogenic perturbation to Mo at the global level and from local observations. We explored, for the first time, the spatial distribution of current atmospheric Mo, and estimate from a combination of observations and modeling that about two-thirds of current atmospheric Mo sources are from anthropogenic sources (14.3 Gg Mo yr^{-1}) compared to natural sources (8.77 Gg Mo yr^{-1}). In industrialized regions, deposition may have increased by 100x or more from combustion of coal and smelting operations. There are large uncertainties in these estimates, suggesting that anthropogenic sources represent between 40 and 75% of the total sources of Mo. Our modeling of Mo deposition did not capture the spatial distribution of either PM_{10} or $PM_{2.5}$, so future studies could improve the simulations. However, given the low concentrations of Mo in the atmosphere and the limited understanding of Mo sources, this study represents an important step forward in understanding Mo cycling. Future studies should focus on refining the role of mining and smelting, especially as the energy transition to renewables is likely to require more

673 Mo and other metals. Finally, the substantial changes in Mo deposition from human activity may
674 affect N cycling differently across ecosystem types.
675
676 **Acknowledgments, Samples, and Data**
677 We acknowledge the Atkinson Center for a Sustainable Future at Cornell University for
678 funding for this project, and thank Adina Paytan for comments on an earlier version of this
679 manuscript. Simulations were undertaken at the NCAR facility (National Center for Atmospheric
680 Research, 2019). We acknowledge many observational networks and sites that were used in this
681 study, including, but not limited to APAD and ASFID: Airborne Particulate Matter Databases
682 Related to the Asia-Pacific Region (http://www.ansto.gov.au/aspdatabases), DEFRA (https://uk-
683 air.defra.gov.uk), the European Monitoring and Evaluation Programme (https://www.emep.int/),
684 the Ministerio del Medio Ambiente de Chile (https://mma.gob.cl), and the Research State
685 Agency of Spain. Houston area measurements were made possible by funding from the Texas
686 Air Research Center and the Texas Commission on Environmental Quality to S. Chellam. F.
687 Lambert acknowledges support from projects ANID/Fondecyt 1191223, ANID/Fondap
688 15110009, and ANID/Millennium Science Initiative/Millennium Nucleus Paleoclimate
689 NCN17_079. N.M. Mahowald acknowledges support from NSF CCF-1522054 and DE-
690 SC0006791. Observational synthesis available in the supplemental materials, while model results
691 are available at the Cornell eCommons repository (https://doi.org/10.7298/nzhv-4579).

692 **References**

693 Adebiyi, A. A., & Kok, J. F. (2020). Climate models miss most of the coarse dust in the
694 atmosphere. *Science Advances*, *6*(15), 1–10. https://doi.org/10.1126/sciadv.aaz9507
695 Alastuey, A., Querol, X., Aas, W., Lucarelli, F., Pérez, N., Moreno, T., et al. (2016).
696 Geochemistry of PM_{10} over Europe during the EMEP intensive measurement periods in
697 summer 2012 and winter 2013. *Atmospheric Chemistry and Physics*, *16*(10), 6107–6129.
698 https://doi.org/10.5194/acp-16-6107-2016
699 Albani, S., Mahowald, N., Perry, A., Scanza, R., Zender, C., & Flanner, M. G. (2014). Improved
700 representation of dust size and optics in the CESM. *Journal of Advances in Modeling of*
701 *Earth Systems*, *6*, doi:10.1002/2013MS000279.
702 Alonso-Hernández, C. M., Bernal-Castillo, J., Bolanos-Alvarez, Y., Gómez-Batista, M., & Diaz-
703 Asencio, M. (2011). Heavy metal content of bottom ashes from a fuel oil power plant and
704 oil refinery in Cuba. *Fuel*, *90*(8), 2820–2823. https://doi.org/10.1016/j.fuel.2011.03.014
705 Alves, C. A., Gomes, J., Nunes, T., Duarte, M., Calvo, A., Custódio, D., et al. (2015). Size-
706 segregated particulate matter and gaseous emissions from motor vehicles in a road tunnel.
707 *Atmospheric Research*, *153*, 134–144. https://doi.org/10.1016/j.atmosres.2014.08.002
708 Amato, F., Moreno, T., Pandolfi, M., Querol, X., Alastuey, A., Delgado, A., et al. (2010).
709 Concentrations, sources and geochemistry of airborne particulate matter at a major
710 European airport. *Journal of Environmental Monitoring*, *12*(4), 854–62.
711 https://doi.org/10.1039/b925439k
712 Andela, N., Morton, D. C., Giglio, L., Chen, Y., Van Der Werf, G. R., Kasibhatla, P. S., et al.
713 (2017). A human-driven decline in global burned area. *Science*, *356*(6345), 1356–1362.
714 https://doi.org/10.1126/science.aal4108

715 Andreae, M. O., & Merlet, P. (2001). Emission of trace gases and aerosols from biomass
716 burning. *Global Biogeochemical Cycles*, *15*(4), 955–966. https://doi.org/10.5194/acp-11-
717 4039-2011
718 Andreae, T. W. (2002). Light scattering by dust and anthropogenic aerosol at a remote site in the
719 Negev desert, Israel. *Journal of Geophysical Research*, *107*(D2), 4008.
720 https://doi.org/10.1029/2001JD900252
721 Atanacio, A. J., & Cohen, D. D. (2020). The IAEA/RCA Fine and Coarse PMF Receptor
722 Fingerprint Database. http://www.ansto.gov.au/aspdatabases
723 Barraza, F., Lambert, F., Jorquera, H., Villalobos, A. M., & Gallardo, L. (2017). Temporal
724 evolution of main ambient PM 2. 5 sources in Santiago, Chile, from 1998 to 2012.
725 *Atmospheric Chemistry and Physics*, *17*(16), 10093–10107. https://doi.org/10.5194/acp-17-
726 10093-2017
727 Barron, A. R., Wurzburger, N., Bellenger, J. P., Wright, S. J., Kraepiel, A. M. L., & Hedin, L. O.
728 (2009). Molybdenum limitation of asymbiotic nitrogen fixation in tropical forest soils.
729 *Nature Geoscience*, *2*(1), 42–45. https://doi.org/10.1038/ngeo366
730 Batjes, N. H. (1997). A world dataset of derived soil properties by FAO-UNESCO soil unit for
731 global modelling. *Soil Use and Management*, *13*(1), 9–16. https://doi.org/10.1111/j.1475-
732 2743.1997.tb00550.x
733 Batterman, S. A., Hedin, L. O., Van Breugel, M., Ransijn, J., Craven, D. J., & Hall, J. S. (2013).
734 Key role of symbiotic dinitrogen fixation in tropical forest secondary succession. *Nature*,
735 *502*(7470), 224–227. https://doi.org/10.1038/nature12525
736 Bauters, M., Drake, T. W., Verbeeck, H., Bodé, S., Hervé-Fernández, P., Zito, P., et al. (2018).
737 High fire-derived nitrogen deposition on central African forests. *Proceedings of the*

738 *National Academy of Sciences of the United States of America*, *115*(3), 549–554.
739 https://doi.org/10.1073/pnas.1714597115
740 Begara-Morales, J. C., Chaki, M., Valderrama, R., Mata-Pérez, C., Padilla-Serrano, M. N., &
741 Barroso, J. B. (2020). Nitric oxide under abiotic stress conditions. *Plant Life Under*
742 *Changing Environment*, 735–754. https://doi.org/10.1016/b978-0-12-818204-8.00032-1
743 Betancourt, D. A., Loveless, T. M., Brown, J. W., & Bishop, P. E. (2008). Characterization of
744 diazotrophs containing Mo-independent nitrogenases, isolated from diverse natural
745 environments. *Applied and Environmental Microbiology*, *74*(11), 3471–3480.
746 https://doi.org/10.1128/AEM.02694-07
747 Bond, T. C., Streets, D. G., Yarber, K. F., Nelson, S. M., Woo, J.-H., & Klimont, Z. (2004). A
748 technology-based global inventory of black and organic carbon emissions from combustion.
749 *Journal of Geophysical Research*, *109*(D14203), doi:10.1029/2003JD003697.
750 Van den Boogaart, K., Tolosana-Delgado, R., & Bren, M. (2014). Compositions: Compositional
751 Data Analysis. R package version 1.40-1. https://CRAN.R-
752 project.org/package=compositions.
753 Boonpeng, C., Polyiam, W., Sriviboon, C., Sangiamdee, D., Watthana, S., Nimis, P. L., &
754 Boonpragob, K. (2017). Airborne trace elements near a petrochemical industrial complex in
755 Thailand assessed by the lichen *Parmotrema tinctorum* (Despr. ex Nyl.) Hale.
756 *Environmental Science and Pollution Research*, *24*(13), 12393–12404.
757 https://doi.org/10.1007/s11356-017-8893-9
758 Bozlaker, A., Prospero, J. M., Price, J., & Chellam, S. (2019). Identifying and Quantifying the
759 Impacts of Advected North African Dust on the Concentration and Composition of
760 Airborne Fine Particulate Matter in Houston and Galveston, Texas. *Journal of Geophysical*

Research: Atmospheres, 1–19. https://doi.org/10.1029/2019JD030792

Bozlaker, A., Buzcu-Güven, B., Fraser, M. P., & Chellam, S. (2013). Insights into PM_{10} sources in Houston, Texas: Role of petroleum refineries in enriching lanthanoid metals during episodic emission events. *Atmospheric Environment*, *69*, 109–117. https://doi.org/10.1016/j.atmosenv.2012.11.068

Bozlaker, A., Spada, N. J., Fraser, M. P., & Chellam, S. (2014). Elemental characterization of $PM_{2.5}$ and PM_{10} emitted from light duty vehicles in the Washburn Tunnel of Houston, Texas: Release of rhodium, palladium, and platinum. *Environmental Science and Technology*, *48*(1), 54–62. https://doi.org/10.1021/es4031003

Brahney, J., Mahowald, N., Ward, D. S., Ballantyne, A. P., & Neff, J. C. (2015). Is atmospheric phosphorus pollution altering global alpine Lake stoichiometry? *Global Biogeochemical Cycles*, *29*(9), 1369–1383. https://doi.org/10.1002/2015GB005137

Carling, G. T., Rupper, S. B., Fernandez, D. P., Tingey, D. G., & Harrison, C. B. (2017). Effect of atmospheric deposition and weathering on trace element concentrations in glacial meltwater at Grand Teton National Park, Wyoming, U.S.A. *Arctic, Antarctic, and Alpine Research*, *49*(3), 427–440. https://doi.org/10.1657/AAAR0016.071

Charter, R. A., Tabatabai, M. A., & Schafer, J. W. (1995). Arsenic, molybdenum, selenium, and tungsten contents of distinct fertilizers and phosphate rocks. *Communications in Soil Science and Plant Analysis*, *26*(17–18), 3051–3062. https://doi.org/10.1080/00103629509369508

Computational and Information Systems Laboratory. (2019). Cheyenne: HPE/SGI ICE XA System (NCAR Community Computing). Boulder, CO: National Center for Atmospheric Research. https://doi.org/10.5065/D6RX99HX

784 Dai, A., & Trenberth, K. E. (2002). Estimates of Freshwater Discharge from Continents:
785 Latitudinal and Seasonal Variations. *Journal of Hydrometeorology*, *3*(6), 660–687.
786 https://doi.org/10.1175/1525-7541(2002)003<0660:EOFDFC>2.0.CO;2
787 Danadurai, K. S. K., Chellam, S., Lee, C.-T., & Fraser, M. P. (2011). Trace elemental analysis of
788 airborne particulate matter using dynamic reaction cell inductively coupled plasma – mass
789 spectrometry: Application to monitoring episodic industrial emission events. *Analytica*
790 *Chimica Acta*, *686*(1–2), 40–49. https://doi.org/10.1016/j.aca.2010.11.037
791 Darnajoux, R., Zhang, X., McRose, D. L., Miadlikowska, J., Lutzoni, F., Kraepiel, A. M. L., &
792 Bellenger, J. P. (2017). Biological nitrogen fixation by alternative nitrogenases in boreal
793 cyanolichens: importance of molybdenum availability and implications for current
794 biological nitrogen fixation estimates. *New Phytologist*, *213*(2), 680–689.
795 https://doi.org/10.1111/nph.14166
796 Darnajoux, R., Magain, N., Renaudin, M., Lutzoni, F., Bellenger, J., & Zhang, X. (2019).
797 Molybdenum threshold for ecosystem scale alternative vanadium nitrogenase activity in
798 boreal forests. *Proceedings of the National Academy of Sciences*, *116*(49), 201913314.
799 https://doi.org/10.1073/pnas.1913314116
800 Das, S., & Chellam, S. (2020). Estimating light-duty vehicles' contributions to ambient $PM_{2.5}$
801 and PM_{10} at a near-highway urban elementary school via elemental characterization
802 emphasizing rhodium, palladium, and platinum. *Science of The Total Environment*,
803 *141*(2016), 141268. https://doi.org/10.1016/j.scitotenv.2020.141268
804 Davidson, E. A., de Carvalho, C. J. R., Figueira, A. M., Ishida, F. Y., Ometto, J. P. H. B.,
805 Nardoto, G. B., et al. (2007). Recuperation of nitrogen cycling in Amazonian forests
806 following agricultural abandonment. *Nature*, *447*(7147), 995–998.

https://doi.org/10.1038/nature05900

DEFRA. (2020). UK Air Information Resource Monitoring Data. Retrieved from https://uk-air.defra.gov.uk/data/

Dentener, F., Drevet, J., Lamarque, J. F., Bey, I., Eickhout, B., Fiore, A. M., et al. (2006). Nitrogen and sulfur deposition on regional and global scales: A multimodel evaluation. *Global Biogeochemical Cycles*, *20*(4), 1–21. https://doi.org/10.1029/2005GB002672

Derimian, Y., Karnieli, A., Kaufman, Y. J., Andreae, M. O., Andreae, T. W., Dubovik, O., et al. (2006). Dust and pollution aerosols over the Negev Desert, Israel– Properties, transport and radiative forcing. *Journal Geophysical Research*, *111*(D05205). https://doi.org/doi:10.1029/2005JD006549

Desboeufs, K. V., Sofikitis, A., Losno, R., Colin, J. L., & Ausset, P. (2005). Dissolution and solubility of trace metals from natural and anthropogenic aerosol particulate matter. *Chemosphere*, *58*(2), 195–203. https://doi.org/10.1016/j.chemosphere.2004.02.025

DFM and WSP. (2020). *Diagnóstico de riesgo ambiental, Región de Antofagasta. Componente A) Estudio de Calidad del Aire por Presencia de Material Particulado Sedimentable en la ciudad de Antofagasta*. Antofagasta, Chile. Retrieved from https://mma.gob.cl/antofagasta/

Dillner, A. M., Schauer, J. J., Christensen, W. F., & Cass, G. R. (2005). A quantitative method for clustering size distributions of elements. *Atmospheric Environment*, *39*(8), 1525–1537. https://doi.org/10.1016/j.atmosenv.2004.11.035

Van Dingenen, R., Raes, F., Putaud, J. P., Baltensperger, U., Charron, A., Facchini, M. C., et al. (2004). A European aerosol phenomenology - 1: Physical characteristics of particulate matter at kerbside, urban, rural and background sites in Europe. *Atmospheric Environment*, *38*(16), 2561–2577. https://doi.org/10.1016/j.atmosenv.2004.01.040

Dongarrà, G., Manno, E., Varrica, D., & Vultaggio, M. (2007). Mass levels, crustal component and trace elements in PM_{10} in Palermo, Italy. *Atmospheric Environment*, *41*(36), 7977–7986. https://doi.org/10.1016/j.atmosenv.2007.09.015

Dongarrà, G., Manno, E., Varrica, D., Lombardo, M., & Vultaggio, M. (2010). Study on ambient concentrations of PM_{10}, $PM_{10\text{-}2.5}$, $PM_{2.5}$ and gaseous pollutants. Trace elements and chemical speciation of atmospheric particulates. *Atmospheric Environment*, *44*(39), 5244–5257. https://doi.org/10.1016/j.atmosenv.2010.08.041

Dynarski, K. A., & Houlton, B. Z. (2018). Nutrient limitation of terrestrial free-living nitrogen fixation. *New Phytologist*, *217*(3), 1050–1061. https://doi.org/10.1111/nph.14905

Eady, R. R. (1996). Structure−function relationships of alternative nitrogenases. *Chemical Reviews*, *96*(7), 3013–3030. https://doi.org/10.1021/cr950057h

European Monitoring and Evaluation Programme. (2020). European Monitoring and Evaluation Programme. Retrieved from https://www.emep.int/

Fujiwara, F., Rebagliati, R. J., Dawidowski, L., Gómez, D., Polla, G., Pereyra, V., & Smichowski, P. (2011). Spatial and chemical patterns of size fractionated road dust collected in a megacitiy. *Atmospheric Environment*, *45*(8), 1497–1505. https://doi.org/10.1016/j.atmosenv.2010.12.053

Fuzzi, S., Decesari, S., Facchini, M. C., Cavalli, F., Emblico, L., Mircea, M., et al. (2007). Overview of the inorganic and organic composition of size-segregated aerosol in Rondônia, Brazil, from the biomass-burning period to the onset of the wet season. *Journal of Geophysical Research*, *112*(D1), D01201. https://doi.org/10.1029/2005JD006741

Ge, S., Bai, Z., Liu, W., Zhu, T., Wang, T., Qing, S., & Zhang, J. (2001). Boiler briquette coal versus raw coal: Part I - Stack gas emissions. *Journal of the Air and Waste Management*

Association, *51*(4), 524–533. https://doi.org/10.1080/10473289.2001.10464293

Gelaro, R., McCarty, W., Suárez, M. J., Todling, R., Molod, A., Takacs, L., et al. (2017). The Modern-Era Retrospective Analysis for Research and Applications, *Journal of Climate*, *2*, 5419–5454. https://doi.org/10.1175/JCLI-D-16-0758.1

Gianini, M. F. D., Gehrig, R., Fischer, A., Ulrich, A., Wichser, A., & Hueglin, C. (2012a). Chemical composition of PM_{10} in Switzerland: An analysis for 2008/2009 and changes since 1998/1999. *Atmospheric Environment*, *54*, 97–106. https://doi.org/10.1016/j.atmosenv.2012.02.037

Gianini, M. F. D., Fischer, A., Gehrig, R., Ulrich, A., Wichser, A., Piot, C., et al. (2012b). Comparative source apportionment of PM_{10} in Switzerland for 2008/2009 and 1998/1999 by Positive Matrix Factorisation. *Atmospheric Environment*, *54*, 149–158. https://doi.org/10.1016/j.atmosenv.2012.02.036

Ginoux, P., Prospero, J. M., Gill, T. E., Hsu, N. C., & Zhao, M. (2012). Global-scale attribution of anthropogenic and natural dust sources and their emission rates based on MODIS Deep Blue aerosol products. *Reviews of Geophysics*, *50*(3), 1–36. https://doi.org/10.1029/2012RG000388

Glass, J. B., Axler, R. P., Chandra, S., & Goldman, C. R. (2012). Molybdenum limitation of microbial nitrogen assimilation in aquatic ecosystems and pure cultures. *Frontiers in Microbiology*, *3*(SEP), 1–11. https://doi.org/10.3389/fmicb.2012.00331

Gonet, T., & Maher, B. A. (2019). Airborne, Vehicle-derived Fe-bearing nanoparticles in the urban environment: a review. *Environmental Science and Technology*, *53*(17), 9970–9991. https://doi.org/10.1021/acs.est.9b01505

Graham, B., Guyon, P., Maenhaut, W., Taylor, P. E., Ebert, M., Matthias-Maser, S., et al. (2003).

876 Composition and diurnal variability of the natural Amazonian aerosol. *Journal of*
877 *Geophysical Research*, *108*(D24), 4765, doi:10.1029/2003JD004049.
878 Grigoratos, T., & Martini, G. (2014). *Non-exhaust traffic related emissions. Brake and tyre wear*
879 *PM*. JRC Science and Policy Reports. https://doi.org/10.2790/21481
880 Grigoratos, T., & Martini, G. (2015). Brake wear particle emissions: a review. *Environmental*
881 *Science and Pollution Research*, *22*(4), 2491–2504. https://doi.org/10.1007/s11356-014-
882 3696-8
883 Hand, J. L., Gill, T. E., & Schichtel, B. A. (2017). Spatial and seasonal variability in fine mineral
884 dust and coarse aerosol mass at remote sites across the United States. *Journal of*
885 *Geophysical Research*, *122*(5), 3080–3097. https://doi.org/10.1002/2016JD026290
886 Hand, J. L., Gill, T. E., & Schichtel, B. A. (2019). Urban and rural coarse aerosol mass across the
887 United States: Spatial and seasonal variability and long-term trends. *Atmospheric*
888 *Environment*, *218*(September), 117025. https://doi.org/10.1016/j.atmosenv.2019.117025
889 Hansen, M. C., Potapov, P. V., Moore, R., Hancher, M., Turubanova, S. A., Tyukavina, A., et al.
890 (2013). High-Resolution Global Maps of 21st-Century Forest Cover Change. *Science*,
891 *342*(November), 850–854. https://doi.org/10.1126/science.1244693
892 Harrison, R. M., Jones, A. M., Gietl, J., Yin, J., & Green, D. C. (2012). Estimation of the
893 contributions of brake dust, tire wear, and resuspension to nonexhaust traffic particles
894 derived from atmospheric measurements. *Environmental Science and Technology*, *46*(12),
895 6523–6529. https://doi.org/10.1021/es300894r
896 Heimburger, A., Losno, R., Triquet, S., Dulac, F., & Mahowald, N. (2012). Direct measurement
897 of atmospheric iron, cobalt and aluminum-derived dust deposition at Kerguelen Islands.
898 *Global Biogeochemical Cycles*, *26*(4), doi:10.1029/2012GB004301.

899 https://doi.org/10.1029/2012GB004301

900 Hernández-Pellón, A., & Fernández-Olmo, I. (2019). Airborne concentration and deposition of
901 trace metals and metalloids in an urban area downwind of a manganese alloy plant.
902 *Atmospheric Pollution Research*, *10*(3), 712–721. https://doi.org/10.1016/j.apr.2018.11.009

903 Houlton, B. Z., Wang, Y.-P., Vitousek, P. M., & Field, C. B. (2008). A unifying framework for
904 dinitrogen fixation in the terrestrial biosphere. *Nature*, *454*(7202), 327–30.
905 https://doi.org/10.1038/nature07028

906 Hsu, C. Y., Chiang, H. C., Lin, S. L., Chen, M. J., Lin, T. Y., & Chen, Y. C. (2016). Elemental
907 characterization and source apportionment of PM_{10} and $PM_{2.5}$ in the western coastal area of
908 central Taiwan. *Science of the Total Environment*, *541*, 1139–1150.
909 https://doi.org/10.1016/j.scitotenv.2015.09.122

910 Hsu, S.-C., Wong, G. T. F., Gong, G.-C., Shiah, F.-K., Huang, Y.-T., Kao, S.-J., et al. (2010).
911 Sources, solubility, and dry deposition of aerosol trace elements over the East China Sea.
912 *Marine Chemistry*, *120*(1–4), 116–127. https://doi.org/10.1016/j.marchem.2008.10.003

913 Hueglin, C., Gehrig, R., Baltensperger, U., Gysel, M., Monn, C., & Vonmont, H. (2005).
914 Chemical characterisation of $PM_{2.5}$, PM_{10} and coarse particles at urban, near-city and rural
915 sites in Switzerland. *Atmospheric Environment*, *39*(4), 637–651.
916 https://doi.org/10.1016/j.atmosenv.2004.10.027

917 Hulskotte, J. H. J., Roskam, G. D., & Denier van der Gon, H. A. C. (2014). Elemental
918 composition of current automotive braking materials and derived air emission factors.
919 *Atmospheric Environment*, *99*, 436–445. https://doi.org/10.1016/j.atmosenv.2014.10.007

920 Hungate, B. A., Stiling, P. D., Dijkstra, P., Johnson, D. W., Ketterer, M. E., Hymus, G. J., et al.
921 (2004). CO_2 elicits long-term decline in nitrogen fixation. *Science*, *304*(5675), 1291.

https://doi.org/10.1126/science.1095549

Hurrell, J. W., Holland, M. M., Gent, P. R., Ghan, S., Kay, J. E., Kushner, P. J., et al. (2013). The community earth system model: A framework for collaborative research. *Bulletin of the American Meteorological Society*, *94*(9). https://doi.org/10.1175/BAMS-D-12-00121.1

Hurtt, G. C., Chini, L. P., Frolking, S., Betts, R. A., Feddema, J., Fischer, G., et al. (2011). Harmonization of land-use scenarios for the period 1500-2100: 600 years of global gridded annual land-use transitions, wood harvest, and resulting secondary lands. *Climatic Change*, *109*(1–2), 117–161, doi:10.1007/s10584-011-0153–2.

Izquierdo, M., & Querol, X. (2012). Leaching behaviour of elements from coal combustion fly ash: An overview. *International Journal of Coal Geology*, *94*, 54–66. https://doi.org/10.1016/j.coal.2011.10.006

Jang, H. N., Seo, Y. C., Lee, J. H., Hwang, K. W., Yoo, J. I., Sok, C. H., & Kim, S. H. (2007). Formation of fine particles enriched by V and Ni from heavy oil combustion: Anthropogenic sources and drop-tube furnace experiments. *Atmospheric Environment*, *41*(5), 1053–1063. https://doi.org/10.1016/j.atmosenv.2006.09.011

Kauffman, J. B., Cummings, D. L., Ward, D. E., & Babbitt, R. (1995). Fire in the Brazilian Amazon: 1. Biomass, nutrient pools, and losses in slashed primary forests. *Oecologia*, *104*(4), 397–408. https://doi.org/10.1007/BF00341336

Kok, J. F., Mahowald, N. M., Fratini, G., Gillies, J. A., Ishizuka, M., Leys, J. F., et al. (2014). An improved dust emission model - Part 1: Model description and comparison against measurements. *Atmospheric Chemistry and Physics*, *14*(23), 13023–13041. https://doi.org/10.5194/acp-14-13023-2014

Kok, Jasper F., Ridley, D. A., Zhou, Q., Miller, R. L., Zhao, C., Heald, C. L., et al. (2017).

945 Smaller desert dust cooling effect estimated from analysis of dust size and abundance.
946 *Nature Geoscience*, *10*(4), 274–278. https://doi.org/10.1038/ngeo2912
947 Laing, J. R., Hopke, P. K., Hopke, E. F., Husain, L., Dutkiewicz, V. A., Paatero, J., & Viisanen,
948 Y. (2013). Long-term trends of biogenic sulfur aerosol and its relationship with sea surface
949 temperature in Arctic Finland. *Journal of Geophysical Research: Atmospheres*, *118*(20),
950 11,770-11,776. https://doi.org/10.1002/2013JD020384
951 Laing, J. R., Hopke, P. K., Hopke, E. F., Husain, L., Dutkiewicz, V. A., Paatero, J., & Viisanen,
952 Y. (2014a). Long-term particle measurements in finnish arctic: Part I - Chemical
953 composition and trace metal solubility. *Atmospheric Environment*, *88*, 275–284.
954 https://doi.org/10.1016/j.atmosenv.2014.03.002
955 Laing, J. R., Hopke, P. K., Hopke, E. F., Husain, L., Dutkiewicz, V. A., Paatero, J., & Viisanen,
956 Y. (2014b). Long-term particle measurements in finnish arctic: Part II - trend analysis and
957 source location identification. *Atmospheric Environment*, *88*, 285–296.
958 https://doi.org/10.1016/j.atmosenv.2014.01.015
959 LeBauer, D. S., & Treseder, K. K. (2008). Nitrogen limitation of net primary productivity in
960 terrestrial ecosystems is globally distributed. *Ecology*, *89*(2), 371–379.
961 https://doi.org/10.1890/06-2057.1
962 Li, L., Mahowald, N., Miller, R. L., Perez Garcia-Pando, C., Klose, M., Hamilton, D. S., et al.
963 (2020). Quantifying the range of the dust direct radiative effect due to source mineralogy
964 uncertainty. *Atmos. Chem. Phys., in Review*.
965 Liu, X., Easter, R. C., Ghan, S. J., Zaveri, R., Rasch, P., Shi, X., et al. (2011). Toward a minimal
966 representation of aerosol direct and indirect effects: model description and evaluation.
967 *Geoscientific Model Development Discussions*, *4*(4), 3485–3598.

https://doi.org/10.5194/gmdd-4-3485-2011

Machado, J. G. M. da S., Brehm, F. A., Moraes, C. A. M., dos Santos, C. A., & Vilela, A. C. F. (2006). Characterization study of electric arc furnace dust phases. *Materials Research*, *9*(1), 41–45. https://doi.org/10.1590/s1516-14392006000100009

Machemer, S. D. (2004). Characterization of airborne and bulk particulate from iron and steel manufacturing facilities. *Environmental Science & Technology*, *38*(2), 381–389. https://doi.org/10.1021/es020897v

Maenhaut, W., Salomonovic, R., Cafmeyer, J., Ichoku, C., Karnieli, A., & Andreae, M. O. (1996a). Anthropogenic and natural radiatively active aerosol types at Sede Boker, Israel. *J. Aerosol Sci.*, *27 (suppl.*, 47–48. https://doi.org/10.1016/0021-8502(96)00096-1

Maenhaut, W., Koppen, G., & Artaxo, P. (1996b). Long-term atmospheric aerosol study in Cuiaba, Brazil: Multielemental composition, sources, and impact of biomass burning. In J. S. Levine (Ed.), *Biomass Burning and Global Change, vol. 2, Biomass Burning in South America, Southeast Asia, and Temperate and Boreal Ecosystems, and the Oil Fires of Kuwait.* (pp. 637–652). Cambridge Massachusetts: MIT Press.

Maenhaut, W., Cafmeyer, J., Ptasinski, J., Andreae, M. O., Andreae, T. W., Elbert, W., et al. (1997a). Chemical composition and light scattering of the atmospheric aerosol at a remote site in the Negev Desert, Israel. *Journal of Aerosol Science*, *28*(Supplement 1), S73–S74. https://doi.org/10.1016/S0021-8502(97)85037-9

Maenhaut, W., Fernandez-Jimenez, M.-T., & Artaxo, P. (1999). Long-term study of atmospheric aerosols in Cuiaba, Brazil: Multielemental composition, sources and source apportionment. *J. Aerosol Sci.*, *30 (suppl.*, 259–260.

Maenhaut, W., Fernandez-Jimenez, M.-T., Vanderzalm, J. L., Hooper, B., Hooper, M. A., &

991 Tapper, N. J. (2000a). Aerosol composition at Jabiru, Australia, and impact of biomass
992 burning,. *J. Aerosol Sci.*, *31 (suppl.*, 745–746. https://doi.org/10.1016/S0021-
993 8502(00)90755-9
994 Maenhaut, W., Fernandez-Jimenez, M.-T.Rajta, Dubtsov, S., Meixner, F. X., Andreae, M. O., et
995 al. (2000b). Long-term aerosol composition measurements and source apportionment at
996 Rukomechi, Zimbabwe. *J. Aerosol Sci.*, *31 (suppl.*, 228–229. https://doi.org/10.1016/S0021-
997 8502(00)90237-4.
998 Maenhaut, W., Ridder, D. J. A. De, Fernandez-Jimenez, M.-T., A., M. H., Hooper, B., &
999 Nurhayati, M. (2002a). Long-term observations of regional aerosol composition at two sites
1000 in Indonesia. *Nucl. Instrum. Methods Phys. Res., Sect. B.*, *189*, 259–265.
1001 https://doi.org/10.1016/S0168- 583X(01)01054-0.
1002 Maenhaut, W, Francois, F., Cafmeyer, J., Gilot, C., & Hanssen, J. E. (1997b). Long-term aerosol
1003 study in southern Norway, and the relationship of aerosol components to source regions. In
1004 P. M. Borrell (Ed.), *Proceedings of Eurotrac Symposium '96 - Transport and*
1005 *Transformation of Pollutants in the Troposphere, Vol 1: Clouds, Aerosols, Modelling and*
1006 *Photo-Oxidants* (pp. 277–280). South Hampton, UK: Computational Mechanics.
1007 Maenhaut, W., & Cafmeyer, J. (1998). Long-Term Atmospheric Aerosol Study at Urban and
1008 Rural Sites in Belgium Using Multi-Elemental Analysis by Particle-Induced X-Ray
1009 Emission Spectrometry and Short-Irradiation Instrumental Neutron Activation Analysis. *X-*
1010 *Ray Spectrometry*, *27*(4), 236–246. https://doi.org/10.1002/(SICI)1097-
1011 4539(199807/08)27:4<236::AID-XRS292>3.0.CO;2-F
1012 Maenhaut, W., Salma, I., Cafmeyer, J., Annegarn, H. J., & Andreae, M. O. (1996c). Regional
1013 atmospheric aerosol composition and sources in the eastern Transvaal, South Africa, and

impact of biomass burning. *Journal of Geophysical Research Atmospheres*, *101*(19), 23631–23650. https://doi.org/10.1029/95jd02930

Maenhaut, W., Fernández-Jiménez, M. T., Rajta, I., & Artaxo, P. (2002b). Two-year study of atmospheric aerosols in Alta Floresta, Brazil: Multielemental composition and source apportionment. *Nuclear Instruments and Methods in Physics Research, Section B: Beam Interactions with Materials and Atoms*, *189*(1–4), 243–248. https://doi.org/10.1016/S0168-583X(01)01050-3

Maenhaut, Willy, Raes, N., Chi, X., Cafmeyer, J., Wang, W., & Salma, I. (2005). Chemical composition and mass closure for fine and coarse aerosols at a kerbside in Budapest, Hungary, in spring 2002. *X-Ray Spectrometry*, *34*(4), 290–296. https://doi.org/10.1002/xrs.820

Maenhaut, Willy, Raes, N., Chi, X., Cafmeyer, J., & Wang, W. (2008). Chemical composition and mass closure for $PM_{2.5}$ and PM_{10} aerosols at K-puszta, Hungary, in summer 2006. *X-Ray Spectrometry*, *37*(2), 193–197. https://doi.org/10.1002/xrs.1062

Maenhaut, Willy, Nava, S., Lucarelli, F., Wang, W., Chi, X., & Kulmala, M. (2011). Chemical composition, impact from biomass burning, and mass closure for $PM_{2.5}$ and PM_{10} aerosols at Hyytiälä, Finland, in summer 2007. *X-Ray Spectrometry*, *40*(3), 168–171. https://doi.org/10.1002/xrs.1302

Mahowald, N., Albani, S., Kok, J. F., Engelstaeder, S., Scanza, R., Ward, D. S., & Flanner, M. G. (2014). The size distribution of desert dust aerosols and its impact on the Earth system. *Aeolian Research*, *15*. https://doi.org/10.1016/j.aeolia.2013.09.002

Mahowald, N. M., Artaxo, P., Baker, A. R., Jickells, T. D., Okin, G. S., Randerson, J. T., & Townsend, A. R. (2005). Impacts of biomass burning emissions and land use change on

1037 Amazonian atmospheric phosphorus cycling and deposition. *Global Biogeochemical*
1038 *Cycles*, *19*(GB4030), 1–15. https://doi.org/10.1029/2005GB002541
1039 Mahowald, N., Jickells, T. D., Baker, A. R., Artaxo, P., Benitez-Nelson, C. R., Bergametti, G., et
1040 al. (2008). Global distribution of atmospheric phosphorus sources, concentrations and
1041 deposition rates, and anthropogenic impacts. *Global Biogeochemical Cycles*, *22*(4), 1–19.
1042 https://doi.org/10.1029/2008GB003240
1043 Mahowald, N., Ward, D. S., Kloster, S., Flanner, M. G., Heald, C. L., Heavens, N. G., et al.
1044 (2011). Aerosol Impacts on Climate and Biogeochemistry. *Annual Review of Environment*
1045 *and Resources*, *36*, 45–74. https://doi.org/10.1146/annurev-environ-042009-094507
1046 Van Marle, M. J. E., Kloster, S., Magi, B. I., Marlon, J. R., Daniau, A. L., Field, R. D., et al.
1047 (2017). Historic global biomass burning emissions for CMIP6 (BB4CMIP) based on
1048 merging satellite observations with proxies and fire models (1750-2015). *Geoscientific*
1049 *Model Development*, *10*(9), 3329–3357. https://doi.org/10.5194/gmd-10-3329-2017
1050 Martin, J., & Meybeck, M. (1979). Elemental Mass-Balance of Material Carried by Major World
1051 Rivers. *Marine Chemistry*, *7*, 173–206.
1052 McRose, D. L., Zhang, X., Kraepiel, A. M. L., & Morel, F. M. M. (2017). Diversity and activity
1053 of alternative nitrogenases in sequenced genomes and coastal environments. *Frontiers in*
1054 *Microbiology*, *8*(FEB), 1–13. https://doi.org/10.3389/fmicb.2017.00267
1055 Meij, R. (1994). Trace element behavior in coal-fired power plants. *Fuel Processing Technology*,
1056 *39*(1–3), 199–217.
1057 De Mello, L. F., Baldanza, M. A. S., Noronha, F. B., & Schmal, M. (2003). NO reduction with
1058 ethanol on MoO_3/Al_2O_3 and CeO_2-ZrO_2-supported Pd catalysts. *Catalysis Today*, *85*(1), 3–
1059 12. https://doi.org/10.1016/S0920-5861(03)00188-3

1060 Meskhidze, N., Chameides, W. L., & Nenes, A. (2005). Dust and pollution: A recipe for
1061 enhanced ocean fertilization? *Journal of Geophysical Research D: Atmospheres*, *110*(3), 1–
1062 23. https://doi.org/10.1029/2004JD005082
1063 Mkoma, S. L., Maenhaut, W., Chi, X., Wang, W., & Raes, N. (2009a). Characterisation of PM_{10}
1064 atmospheric aerosols for the wet season 2005 at two sites in East Africa. *Atmospheric*
1065 *Environment*, *43*(3), 631–639. https://doi.org/10.1016/j.atmosenv.2008.10.008
1066 Mkoma, S. L., Maenhaut, W., Chi, X., Wang, W., & Raes, N. (2009b). Chemical composition
1067 and mass closure for PM_{10} aerosols during the 2005 dry season at a rural site in Morogoro,
1068 Tanzania. *X-Ray Spectrometry*, *38*(4), 293–300. https://doi.org/10.1002/xrs.1179
1069 Mkoma, S. L., Wang, W., & Maenhaut, W. (2009c). Seasonal variation of water-soluble
1070 inorganic species in the coarse and fine atmospheric aerosols at Dar es Salaam, Tanzania.
1071 *Nuclear Instruments and Methods in Physics Research, Section B: Beam Interactions with*
1072 *Materials and Atoms*, *267*(17), 2897–2902. https://doi.org/10.1016/j.nimb.2009.06.099
1073 Moreno, N., Querol, X., Andres, J. M., Stanton, K., Towler, M., Nugteren, H., et al. (2005).
1074 Physico-chemical characteristics of European pulverized coal combustion fly ashes. *Fuel*,
1075 *84*(11), 1351–1363. https://doi.org/10.1016/j.fuel.2004.06.038
1076 Morera-Gómez, Y., Elustondo, D., Lasheras, E., Alonso-Hernández, C. M., & Santamaría, J. M.
1077 (2018). Chemical characterization of PM_{10} samples collected simultaneously at a rural and
1078 an urban site in the Caribbean coast: Local and long-range source apportionment.
1079 *Atmospheric Environment*, *192*(August), 182–192.
1080 https://doi.org/10.1016/j.atmosenv.2018.08.058
1081 Morera-Gómez, Y., Alonso-Hernández, C. M., Santamaría, J. M., Elustondo, D., Lasheras, E., &
1082 Widory, D. (2020). Levels, spatial distribution, risk assessment, and sources of

environmental contamination vectored by road dust in Cienfuegos (Cuba) revealed by chemical and C and N stable isotope compositions. *Environmental Science and Pollution Research*, *27*(2), 2184–2196. https://doi.org/10.1007/s11356-019-06783-7

NPCS Board of Consultants & Engineers. (2009). *Handbook on Rare Earth Metals and Alloys (Properties, Extraction, Preparation and Applications)*. Asia Pacific Business Press, Inc.

Nriagu, J. O. (1989). A global assessment of natural sources of atmospheric trace metals. *Nature*, *338*(6210), 47–49. https://doi.org/10.1038/338047a0

Nriagu, J. O., & Pacyna, J. M. (1988). Quantitative assessment of worldwide contamination of air, water and soils by trace metals. *Nature*, *333*(6169), 134–139. https://doi.org/10.1038/333134a0

Nyanganyura, D., Maenhaut, W., Mathuthu, M., Makarau, A., & Meixner, F. X. (2007). The chemical composition of tropospheric aerosols and their contributing sources to a continental background site in northern Zimbabwe from 1994 to 2000. *Atmospheric Environment*, *41*(12), 2644–2659. https://doi.org/10.1016/j.atmosenv.2006.11.015

O'Dowd, C. D., & de Leeuw, G. (2007). Marine aerosol production: a review of the current knowledge. *Philosophical Transactions of the Royal Society A: Mathematical, Physical and Engineering Sciences*, *365*(1856), 1753–1774. https://doi.org/10.1098/rsta.2007.2043

Okin, G.S., Mahowald, N., Chadwick, O. A., & Artaxo, P. (2004). Impact of desert dust on the biogeochemistry of phosphorus in terrestrial ecosystems. *Global Biogeochemical Cycles*, *18*(2). https://doi.org/10.1029/2003GB002145

Peñuelas, J., Sardans, J., Rivas-ubach, A., & Janssens, I. A. (2012). The human-induced imbalance between C, N and P in Earth's life system. *Global Change Biology*, *18*(1), 3–6. https://doi.org/10.1111/j.1365-2486.2011.02568.x

Peñuelas, J., Poulter, B., Sardans, J., Ciais, P., Van Der Velde, M., Bopp, L., et al. (2013). Human-induced nitrogen-phosphorus imbalances alter natural and managed ecosystems across the globe. *Nature Communications*, *4*. https://doi.org/10.1038/ncomms3934

Perakis, S. S., Pett-Ridge, J. C., & Catricala, C. E. (2017). Nutrient feedbacks to soil heterotrophic nitrogen fixation in forests. *Biogeochemistry*, *134*(1), 41–55. https://doi.org/10.1007/s10533-017-0341-x

Pérez, N., Pey, J., Querol, X., Alastuey, A., López, J. M., & Viana, M. (2008). Partitioning of major and trace components in PM_{10}-$PM_{2.5}$-PM_1 at an urban site in Southern Europe. *Atmospheric Environment*, *42*(8), 1677–1691. https://doi.org/10.1016/j.atmosenv.2007.11.034

Prospero, J. M., Barrett, K., Church, T., Dentener, F., Duce, R. A., Galloway, J. N., et al. (1996). Atmospheric deposition of nutrients to the North Atlantic Basin. *Biogeochemistry*, *35*(1), 27–73. https://doi.org/10.1007/BF02179824

Putaud, J.-P., Van Dingenen, R., Alastuey, A., Bauer, H., Birmili, W., Cyrys, J., et al. (2010). A European aerosol phenomenology – 3: Physical and chemical characteristics of particulate matter from 60 rural, urban, and kerbside sites across Europe. *Atmospheric Environment*, *44*(10), 1308–1320. https://doi.org/10.1016/j.atmosenv.2009.12.011

Putaud, J-P, Raes, F., Van Dingenen, R., Brüggemann, E., Facchini, M.-C., Decesari, S., et al. (2004). A European aerosol phenomenology—2: chemical characteristics of particulate matter at kerbside, urban, rural and background sites in Europe. *Atmospheric Environment*, *38*(16), 2579–2595. https://doi.org/10.1016/j.atmosenv.2004.01.041

Qu, Z., Trabelsi, A., Losno, R., Monna, F., Nowak, S., Masmoudi, M., & Quisefit, J. P. (2020). A laboratory dust generator applying vibration to soil sample: mineralogical study and

compositional analyses. *Journal of Geophysical Research: Atmospheres*, *125*(7), 1–10. https://doi.org/10.1029/2019JD032224

Querol, X., Fernández-Turiel, J., & López-Soler, A. (1995). Trace elements in coal and their behaviour during combustion in a large power station. *Fuel*, *74*(3), 331–343. https://doi.org/10.1016/0016-2361(95)93464-O

R Core Team. (2018). R: A language and environment for statistical computing. R Foundation for Statistical Computing, Vienna, Austria.

Rathod, S. D., Hamilton, D. S., & Mahowald, N. M. (n.d.). Constraining present-day aerosol-iron emissions using models and observations. *Journal of Geophysical Research Atmospheres, in Preparation*.

Rathod, S. D., Hamilton, D. S., Mahowald, N. M., Klimont, Z., Corbett, J. J., & Bond, T. C. (2020). A mineralogy-based anthropogenic combustion-iron emission inventory. *Journal of Geophysical Research: Atmospheres*, *125*(17), 1–35. https://doi.org/10.1029/2019JD032114

Rauch, J. N., & Pacyna, J. M. (2009). Earth's global Ag, Al, Cr, Cu, Fe, Ni, Pb, and Zn cycles. *Global Biogeochemical Cycles*, *23*(2), 1–16. https://doi.org/10.1029/2008GB003376

Reed, S. C., Cleveland, C. C., & Townsend, A. R. (2013). Relationships among phosphorus, molybdenum and free-living nitrogen fixation in tropical rain forests: results from observational and experimental analyses. *Biogeochemistry*, *114*(1–3), 135–147. https://doi.org/10.1007/s10533-013-9835-3

Ridley, D. A., Heald, C. L., Kok, J. F., & Zhao, C. (2016). An observationally constrained estimate of global dust aerosol optical depth. *Atmospheric Chemistry and Physics*, *16*(23), 15097–15117. https://doi.org/10.5194/acp-16-15097-2016

Robertson, J. M., Nesbitt, J. A., & Lindsay, M. B. J. (2019). Aqueous- and solid-phase

molybdenum geochemistry of oil sands fluid petroleum coke deposits, Alberta, Canada. *Chemosphere*, *217*, 715–723. https://doi.org/10.1016/j.chemosphere.2018.11.064

Rodríguez, S., Alastuey, A., Alonso-Pérez, S., Querol, X., Cuevas, E., Abreu-Afonso, J., et al. (2011). Transport of desert dust mixed with North African industrial pollutants in the subtropical Saharan Air Layer. *Atmospheric Chemistry and Physics*, *11*(13), 6663–6685. https://doi.org/10.5194/acp-11-6663-2011

Rodríguez, S., Cuevas, E., Prospero, J. M., Alastuey, A., Querol, X., López-Solano, J., et al. (2015). Modulation of Saharan dust export by the North African dipole. *Atmospheric Chemistry and Physics*, *15*(13), 7471–7486. https://doi.org/10.5194/acp-15-7471-2015

Romero, I. C., Klein, N. J., Sañudo-Wilhelmy, S. A., & Capone, D. G. (2013). Potential trace metal co-limitation controls on N_2 fixation and NO_3^- uptake in lakes with varying trophic Status. *Frontiers in Microbiology*, *4*. https://doi.org/10.3389/fmicb.2013.00054

Rousk, K., Degboe, J., Michelsen, A., Bradley, R., & Bellenger, J. (2016). Molybdenum and phosphorus limitation of moss-associated nitrogen fixation in boreal ecosystems. *New Phytologist*, *214*(1), 97–107. https://doi.org/10.1111/nph.14331

Rudnick, R. L., & Gao, S. (2003). Composition of the continental crust. In R. L. Rudnick (Ed.), *The Crust* (pp. 1–64). Elsevier.

Ryder, C. L., Highwood, E. J., Walser, A., Seibert, P., Philipp, A., & Weinzierl, B. (2019). Coarse and Giant Particles are Ubiquitous in Saharan Dust Export Regions and are Radiatively Significant over the Sahara. *Atmospheric Chemistry and Physics Discussions*, (June), 1–36. https://doi.org/10.5194/acp-2019-421

Salma, I., Maenhaut, W., Annegarn, H. J., Andreae, M. O., Meixner, F. X., & Garstang., M. (1997). Combined application of INAA and PIXE for studying the regional aerosol

composition in Southern Africa. *Journal of Geophsyical Research*, *101*, 2361–23650.

Scanza, R. A., Mahowald, N., Ghan, S., Zender, C. S., Kok, J. F., Liu, X., et al. (2015). Modeling dust as component minerals in the Community Atmosphere Model: development of framework and impact on radiative forcing. *Atmospheric Chemistry and Physics*, *15*(1), 537–561. https://doi.org/10.5194/acp-15-537-2015

Schlesinger, W. H., Klein, E. M., & Vengosh, A. (2017). Global biogeochemical cycle of vanadium. *Proceedings of the National Academy of Sciences*, E11092–E11100. https://doi.org/10.1073/pnas.1715500114

Schmal, M., Baldanza, M. A. S., & Vannice, M. A. (1999). Pd-xMo/Al_2O_3 catalysts for NO reduction by CO. *Journal of Catalysis*, *185*(1), 138–151. https://doi.org/10.1006/jcat.1999.2465

Schutgens, N. A. J., Gryspeerdt, E., Weigum, N., Tsyro, S., Goto, D., Schulz, M., & Stier, P. (2016). Will a perfect model agree with perfect observations? The impact of spatial sampling. *Atmospheric Chemistry and Physics*, *16*(10), 6335–6353. https://doi.org/10.5194/acp-16-6335-2016

Sedwick, P. N., Sholkovitz, E. R., & Church, T. M. (2007). Impact of anthropogenic combustion emissions on the fractional solubility of aerosol iron: Evidence from the Sargasso Sea. *Geochemistry, Geophysics, Geosystems*, *8*(10). https://doi.org/10.1029/2007GC001586

Selin, N. E. (2009). Global Biogeochemical Cycling of Mercury: A Review. *Annual Review of Environment and Resources*, *34*(1), 43–63. https://doi.org/10.1146/annurev.environ.051308.084314

Sen, I. S., & Peucker-Ehrenbrink, B. (2012). Anthropogenic Disturbance of Element Cycles at the Earth's Surface. *Environmental Science & Technology*, *46*(16), 8601–8609.

https://doi.org/10.1021/es301261x

Settle, D. M., & Patterson, C. C. (1982). Magnitudes and sources of precipitation and dry deposition fluxes of indestrial and natural leads to the North Pacific at Enewetak. *Journal of Geophysical Research*, *87*(C11), 8857. https://doi.org/10.1029/JC087iC11p08857

da Silva, L. I. D., de Souza Sarkis, J. E., Zotin, F. M. Z., Carneiro, M. C., Neto, A. A., da Silva, A. dos S. A. G., et al. (2008). Traffic and catalytic converter - Related atmospheric contamination in the metropolitan region of the city of Rio de Janeiro, Brazil. *Chemosphere*, *71*(4), 677–684. https://doi.org/10.1016/j.chemosphere.2007.10.057

Silvester, W. B. (1989). Molybdenum limitation of asymbiotic nitrogen fixation in forests of Pacific Northwest America. *Soil Biology and Biochemistry*, *21*(2), 283–289. https://doi.org/10.1016/0038-0717(89)90106-5

Smichowski, P., Gómez, D. R., Dawidowski, L. E., Giné, M. F., Bellato, A. C. S., & Reich, S. L. (2004). Monitoring trace metals in urban aerosols from Buenos Aires city. Determination by plasma-based techniques. *Journal of Environmental Monitoring*, *6*(4), 286–294. https://doi.org/10.1039/b312446k

Spiro, P. A., Jacob, D. J., & Logan, J. A. (1992). Global inventory of sulfur emissions with 1° × 1° resolution. *Journal of Geophysical Research*, *97*(D5), 6023–6036. https://doi.org/10.1029/91JD03139

Swap, R. J., Annegarn, H. J., Suttles, J. T., Haywood, J., Helmlinger, M. C., Hely, C., et al. (2002). The Southern African Regional Science Initiative (SAFARI 2000): Overview of the dry season field campaign. *South African Journal of Science*, *98*(3–4), 125–130.

Sylvestre, A., Mizzi, A., Mathiot, S., Masson, F., Jaffrezo, J. L., Dron, J., et al. (2017). Comprehensive chemical characterization of industrial $PM_{2.5}$ from steel industry activities.

Atmospheric Environment, *152*, 180–190. https://doi.org/10.1016/j.atmosenv.2016.12.032

Taylor, S. R., & McLennan, S. M. (1995). The geochemical evolution of the continental crust. *Reviews of Geophysics*, *33*(2), 241. https://doi.org/10.1029/95RG00262

Thornton, P. E., Doney, S. C., Lindsay, K., Moore, J. K., Mahowald, N., Randerson, J. T., et al. (2009). Carbon-nitrogen interactions regulate climate-carbon cycle feedbacks: results from an atmosphere-ocean general circulation model. *Biogeosciences*, *6*(10), 2099–2120. https://doi.org/10.5194/bg-6-2099-2009

Thorpe, A., & Harrison, R. M. (2008). Sources and properties of non-exhaust particulate matter from road traffic: A review. *Science of the Total Environment*, *400*(1–3), 270–282. https://doi.org/10.1016/j.scitotenv.2008.06.007

Vanderzalm, J. L., Hooper, M. A., Ryan, B., Maenhaut, W., P. Martin, P. R., Rayment, & Hooper, B. M. (2003). Impact of seasonal biomass burning on air quality in the 'Top End' of regional northern Australia. *Clean Air Environ. Qual.*, *37*(3), 28–34.

Virkkula, A., Aurela, M., Hillamo, R., Mäkelä, T., Pakkanen, T., Kerminen, V.-M., et al. (1999). Chemical composition of atmospheric aerosol in the European subarctic: Contribution of the Kola Peninsula smelter areas, central Europe, and the Arctic Ocean. *Journal of Geophysical Research: Atmospheres*, *104*(D19), 23681–23696. https://doi.org/10.1029/1999JD900426

Vitousek, P., & Howarth, R. (1991). Nitrogen limitation on land and in the sea: How can it occur? *Biogeochemistry*, *13*(2), 87–115. https://doi.org/10.1007/BF00002772

Voutsa, D., & Samara, C. (2002). Labile and bioaccessible fractions of heavy metals in the airborne particulate matter from urban and industrial areas. *Atmospheric Environment*, *36*(22), 3583–3590. https://doi.org/10.1016/S1352-2310(02)00282-0

1244 Wang, Y.-P., & Houlton, B. Z. (2009). Nitrogen constraints on terrestrial carbon uptake:
1245 Implications for the global carbon-climate feedback. *Geophysical Research Letters*, *36*(24),
1246 L24403. https://doi.org/10.1029/2009GL041009
1247 van der Werf, G. R., Randerson, J., Collatz, G. J., Giglio, L., Kasibhatla, P., Arrellano, A., et al.
1248 (2004). Continental-scale partitioning of fire emissions during the 1997 to 2001 El Nino/La
1249 Nina Period. *Science*, *303*, 73–76.
1250 Wong, M. Y., Neill, C., Marino, R., Silvério, D., & Howarth, R. W. (2020a). Molybdenum,
1251 phosphorus, and pH do not constrain nitrogen fixation in a tropical forest in the southeastern
1252 Amazon. *Ecology*. https://doi.org/10.1002/ecy.3211
1253 Wong, M. Y., Mahowald, N. M., Marino, R., Williams, E. R., Chellam, S., & Howarth, R. W.
1254 (2020b). Natural atmospheric deposition of molybdenum: a global model and implications
1255 for tropical forests. *Biogeochemistry*, *149*(2), 159–174. https://doi.org/10.1007/s10533-020-
1256 00671-w
1257 Wurzburger, N., Bellenger, J. P., Kraepiel, A. M. L., & Hedin, L. O. (2012). Molybdenum and
1258 phosphorus interact to constrain asymbiotic nitrogen fixation in tropical forests. *PloS ONE*,
1259 *7*(3), 1–7. https://doi.org/10.1371/journal.pone.0033710
1260 Xiao, Y. H., Liu, S. R., Tong, F. C., Kuang, Y. W., Chen, B. F., & Guo, Y. D. (2014).
1261 Characteristics and sources of metals in TSP and $PM_{2.5}$ in an urban forest park at
1262 Guangzhou. *Atmosphere*, *5*(4), 775–787. https://doi.org/10.3390/atmos5040775
1263 Yu, H., Chin, M., Yuan, T., Bian, H., Remer, L. A., Prospero, J. M., et al. (2015). The fertilizing
1264 role of African dust in the Amazon rainforest: A first multiyear assessment based on data
1265 from Cloud-Aerosol Lidar and Infrared Pathfinder Satellite Observations. *Geophysical*
1266 *Research Letters*, *42*(6), 1984–1991. https://doi.org/10.1002/2015GL063040

1267 Zender, C., Bian, H., & Newman, D. (2003). Mineral Dust Entrainment and Deposition (DEAD)
1268 model: Description and 1990s dust climatology. *Journal of Geophysical Research*,
1269 *108*(D14), 4416, doi:10.1029/2002JD002775.
1270 Zhang, X., McRose, D. L., Darnajoux, R., Bellenger, J. P., Morel, F. M. M., & Kraepiel, A. M.
1271 L. (2016). Alternative nitrogenase activity in the environment and nitrogen cycle
1272 implications. *Biogeochemistry*, *127*, 189–198. https://doi.org/10.1007/s10533-016-0188-6
1273 Zheng, M., Zhang, W., Luo, Y., Li, D., Wang, S., Huang, J., et al. (2018). Stoichiometry controls
1274 asymbiotic nitrogen fixation and its response to nitrogen inputs in a nitrogen-saturated
1275 forest. *Ecology*, *99*(9), 2037–2046. https://doi.org/10.1002/ecy.2416
1276 Zheng, M., Zhou, Z., Zhao, P., Luo, Y., Ye, Q., Zhang, K., et al. (2020). Effects of human
1277 disturbance activities and environmental change factors on terrestrial nitrogen fixation.
1278 *Global Change Biology*, *26*(11), 6203–6217. https://doi.org/10.1111/gcb.15328
1279

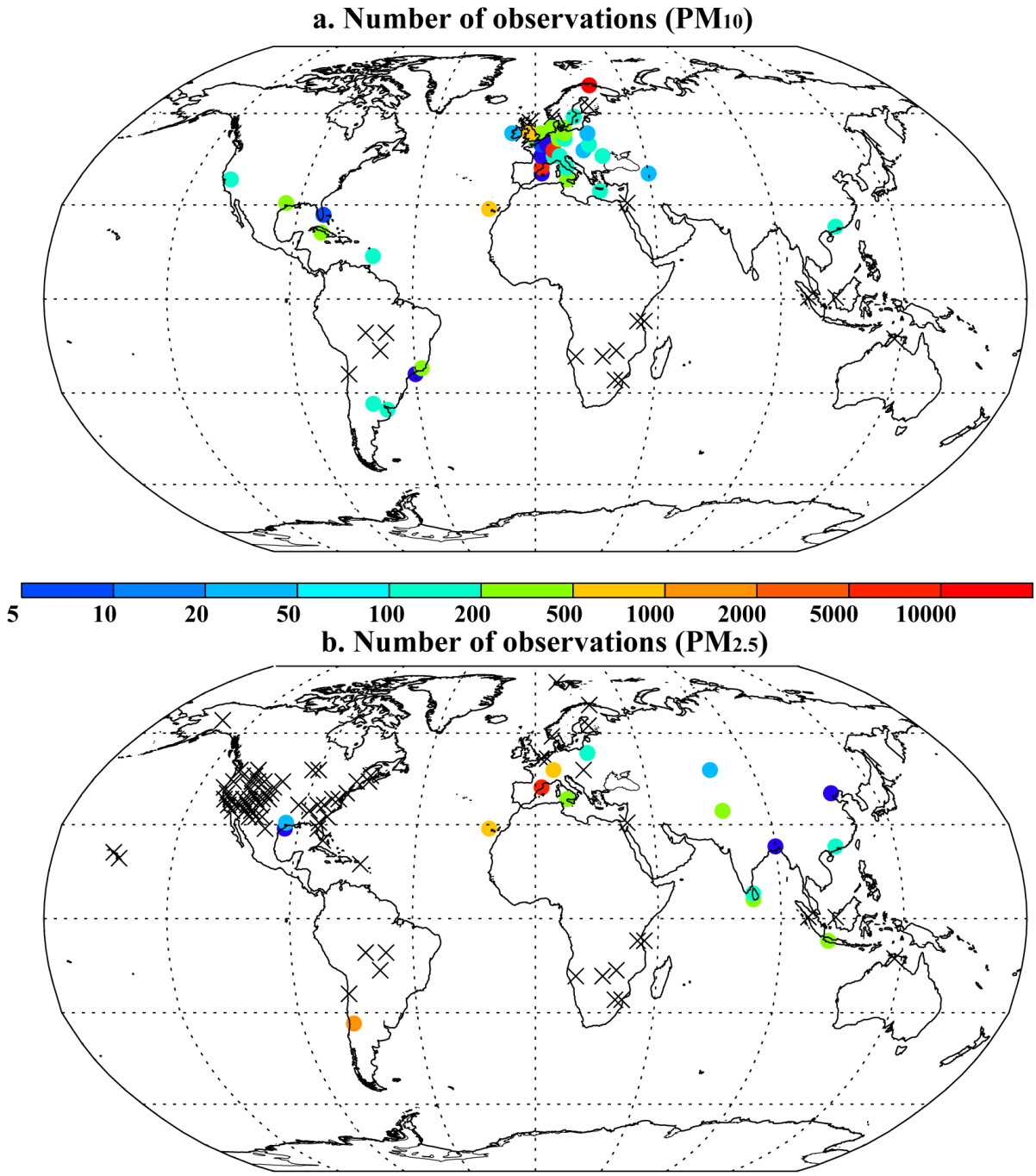

Figure 1. (a) The number of Mo concentration observations (PM_{10}) and (b) the number of number of Mo concentration observations ($PM_{2.5}$) above detection level at each site. Observations collected at sites within a 2°x2° grid box are compiled. Sites with no values above detection levels are represented by an "x." For the sites that measured coarse ($PM_{10-2.5}$) and fine

($PM_{2.5}$) observations instead of $PM_{2.5}$ and PM_{10}, we summed those observations and categorized those sites as PM_{10}. Details on the studies and methods are included in the Supporting Information (Data Set 1) as well as the respective studies (Alastuey et al., 2016; Andreae et al., 2002; Atanacio & Cohen, 2020; Barraza et al., 2017; Bozlaker et al., 2013, 2019; DEFRA, 2020; Derimian et al., 2006; DFM and WSP, 2020; Van Dingenen et al., 2004; Dongarrà et al., 2007, 2010; European Monitoring and Evaluation Programme, 2020; Fuzzi et al., 2007; Gianini et al., 2012a, 2012b; Hand et al., 2017; Hsu et al., 2016; Hueglin et al., 2005; Laing et al., 2014a, 2014b; Maenhaut et al., 1996a, 1996b, 1996c, 1997a, 1997b, 1999, 2000a, 2000b, 2002a, 2002b, 2005, 2008, 2011; Maenhaut & Cafmeyer, 1998; Mkoma et al., 2009a, 2009b, 2009c; Morera-Gómez et al., 2018; Nyanganyura et al., 2007; Pérez et al., 2008; Putaud et al., 2004, 2010; Rodríguez et al., 2011, 2015; Salma et al., 1997; da Silva et al., 2008; Smichowski et al., 2004; Swap et al., 2002; Vanderzalm et al., 2003; Virkkula et al., 1999; Xiao et al., 2014).

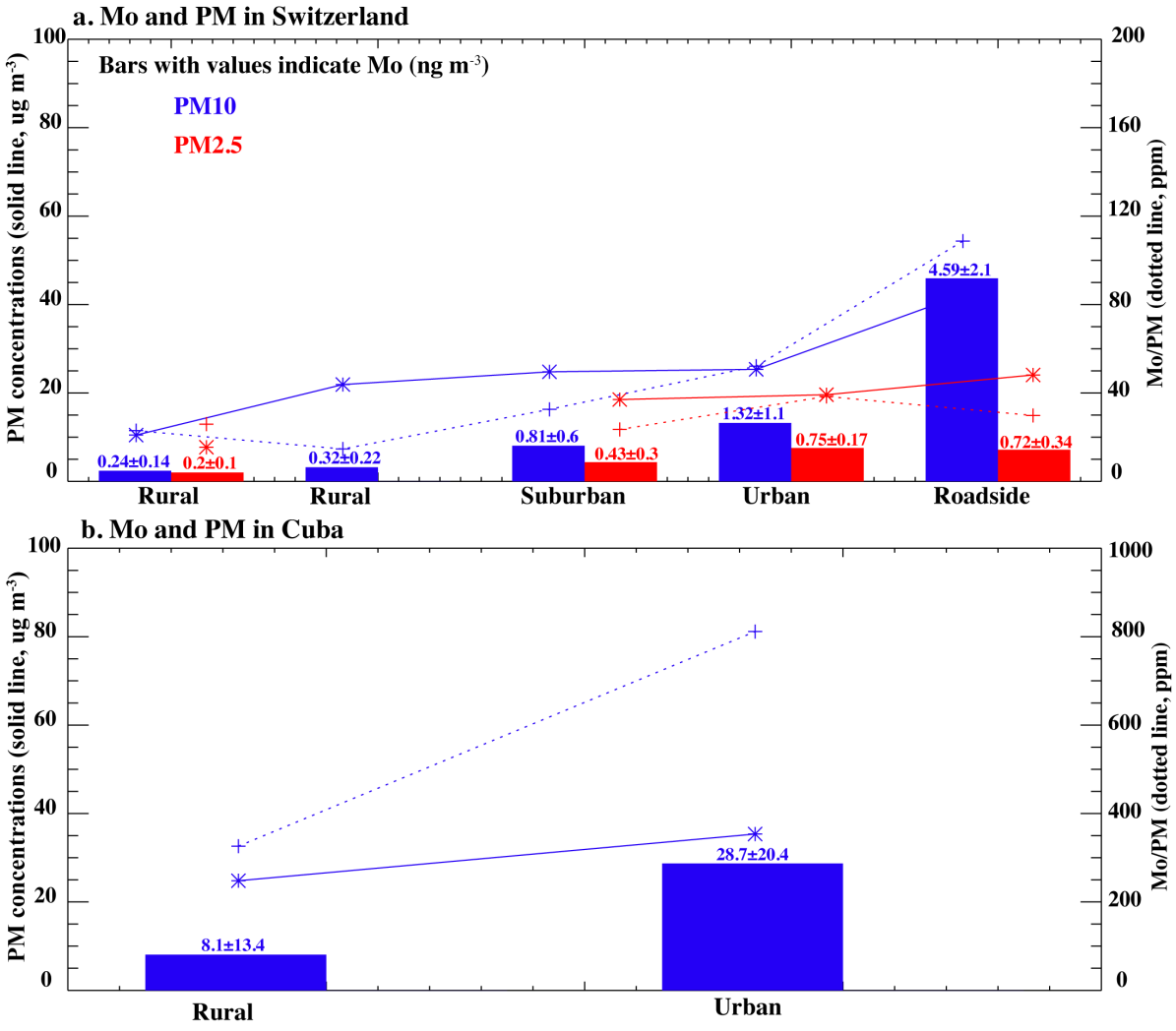

Figure 2. (a) Mo in particulate matter across Switzerland shown in the bars, with the values shown over each bar (ng m^{-3}) in blue (PM_{10}) and red ($PM_{2.5}$) increasing along a gradient towards more urbanized sites (left to right). Similarly the total particulate matter increases in the more urban sites in both PM_{10} (blue) and $PM_{2.5}$ (red) (solid line, µg m^{-3} left hand axis). The fraction of the Mo in PM tends to increase in more urban environments (dotted line, mg Mo kg^{-1}, right hand axis). Data are from Hueglin et al. (2005). (b) Similar for data from Cuba but only for PM_{10}. Note there is much more aerosol and Mo in Cuba than in Switzerland. Data are from Morera-Gómez et al., (2018). The means ± the standard deviations are presented for the Mo

1306 concentrations.

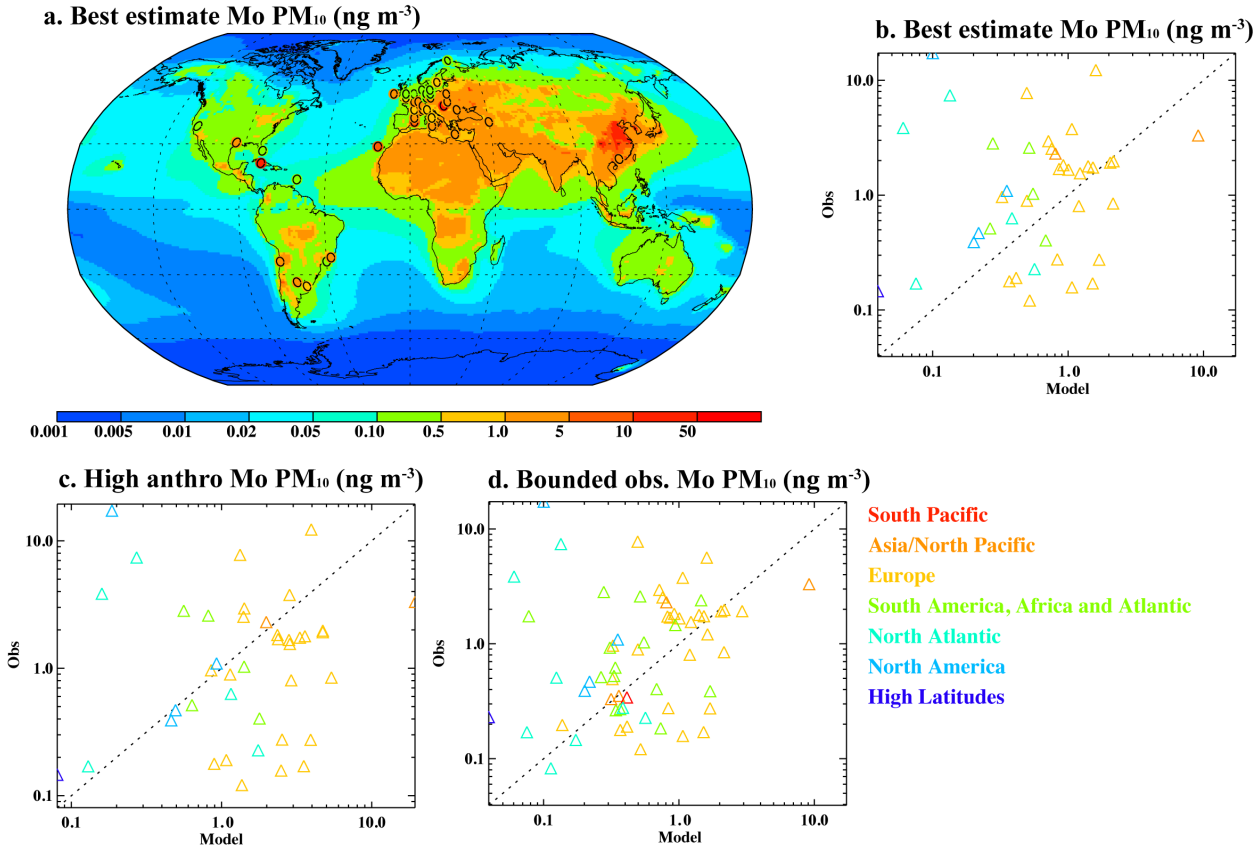

1307

1308 **Figure 3.** (a) Horizontal distribution of the surface concentrations of Mo (ng m^{-3}) in the PM_{10}
1309 size fraction as simulated in the model using the best estimate scenario (contours) and from the
1310 observations (circles). Observations are averaged to a ~2ºx2º grid and compared to Community
1311 Atmosphere Model (CAM) (v6) results. (b) Scatterplot comparison of the modeled simulations
1312 in the best estimate scenario against observations (same as in a) (n=40, r=0.01). (c) Same as (b),
1313 except for the high anthropogenic model case (n=40, r=0.00). (d) Same as in (b), except that all
1314 stations are included, even if more than 50% of the observational values are below the detection
1315 limit to show the upper bound on observations as described in the Methods (n=61, r=0.05). In the
1316 scatter plots, colors indicate locations: South Pacific (red), Asia/North Pacific (orange), Europe
1317 (green), South America, Africa and Atlantic (cyan), North Atlantic (medium blue), North
1318 America (dark blue), High Latitudes (purple).

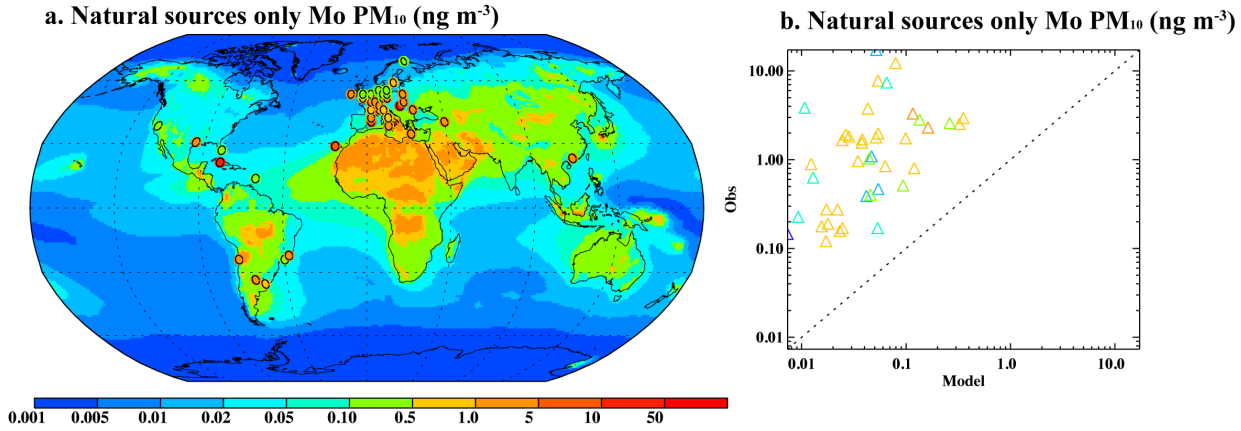

1319

1320 **Figure 4.** (a) Spatial distribution of the surface concentrations of Mo (ng m^{-3}) as simulated in the
1321 Community Atmosphere Model (CAM) (v6) using only natural sources (contours) overlain by
1322 observational data (circles). Observations are averaged to a ~2ºx2º grid and compared to the
1323 model. (b) Scatterplot comparison of the modeled surface concentrations of Mo (ng m^{-3}) in the
1324 natural sources only scenario against observations (same as in (a)) (n=40, r=0.13). In the scatter
1325 plots, colors indicate locations: South Pacific (red), Asia/North Pacific (orange), Europe (green),
1326 South America, Africa and Atlantic (cyan), North Atlantic (medium blue), North America (dark
1327 blue), High Latitudes (purple).

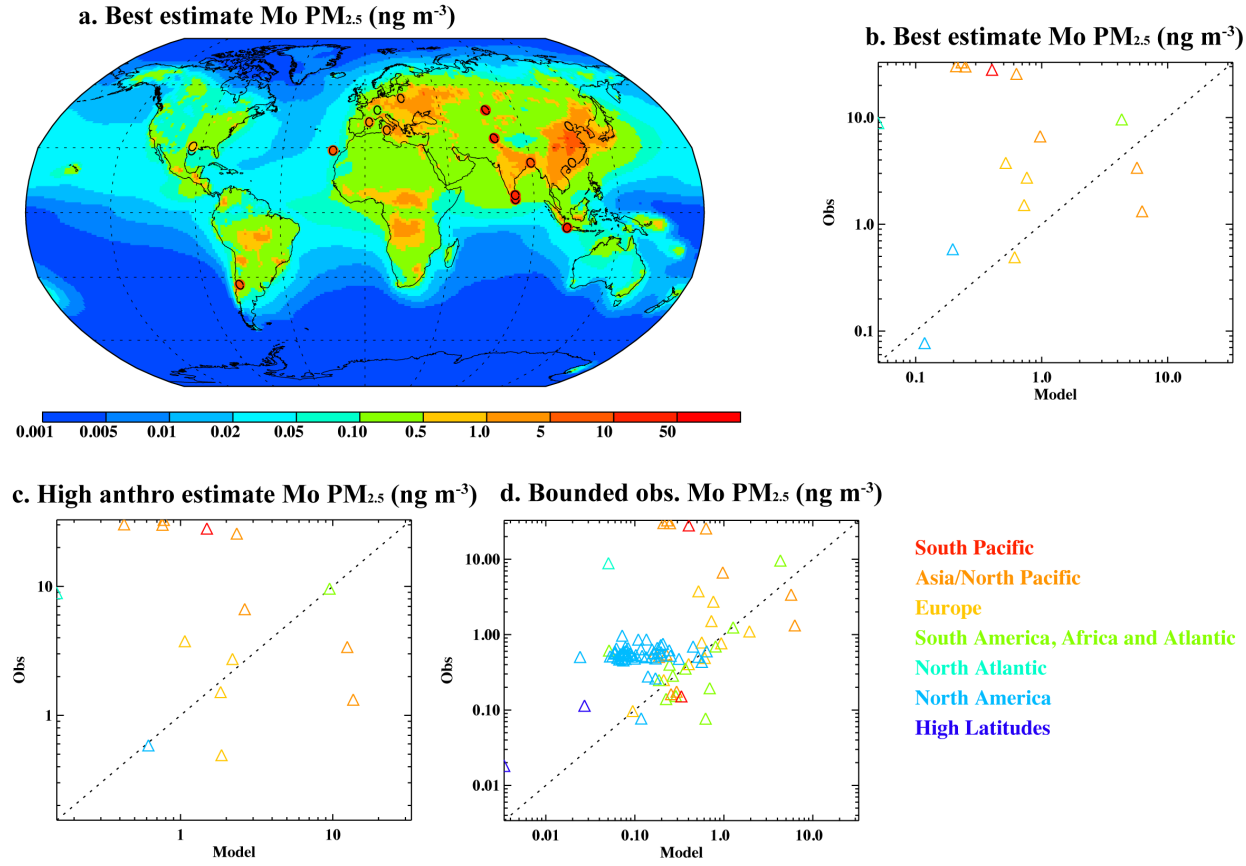

1328

1329 **Figure 5.** (a) Same as Figure 3, but for $PM_{2.5}$. Spatial distribution of the surface concentrations
1330 $PM_{2.5}$ of Mo (ng m^{-3}) as simulated in the Community Atmosphere Model (CAM) (v6) using the
1331 best estimate scenario (contours) and overlain by observational data (circles). Observations are
1332 averaged to a ~2ºx2º grid and compared to the model. (b) Scatterplot comparison of the modeled
1333 surface concentrations $PM_{2.5}$ of Mo (ng m^{-3}) in the best estimate scenario against observations
1334 (same as in a) (n=16, r=-0.32). (c) Same as (b), except for the high anthropogenic model case
1335 (n=16, r=-0.13). (d) Same as in (b), except that all observational values below the detection limit
1336 as included to show the upper bound on observations as described in the Methods (n=93,
1337 r=0.07). In the scatter plots, colors indicate locations: South Pacific (red), Asia/North Pacific

(orange), Europe (green), South America, Africa and Atlantic (cyan), North Atlantic (medium blue), North America (dark blue), High Latitudes (purple).

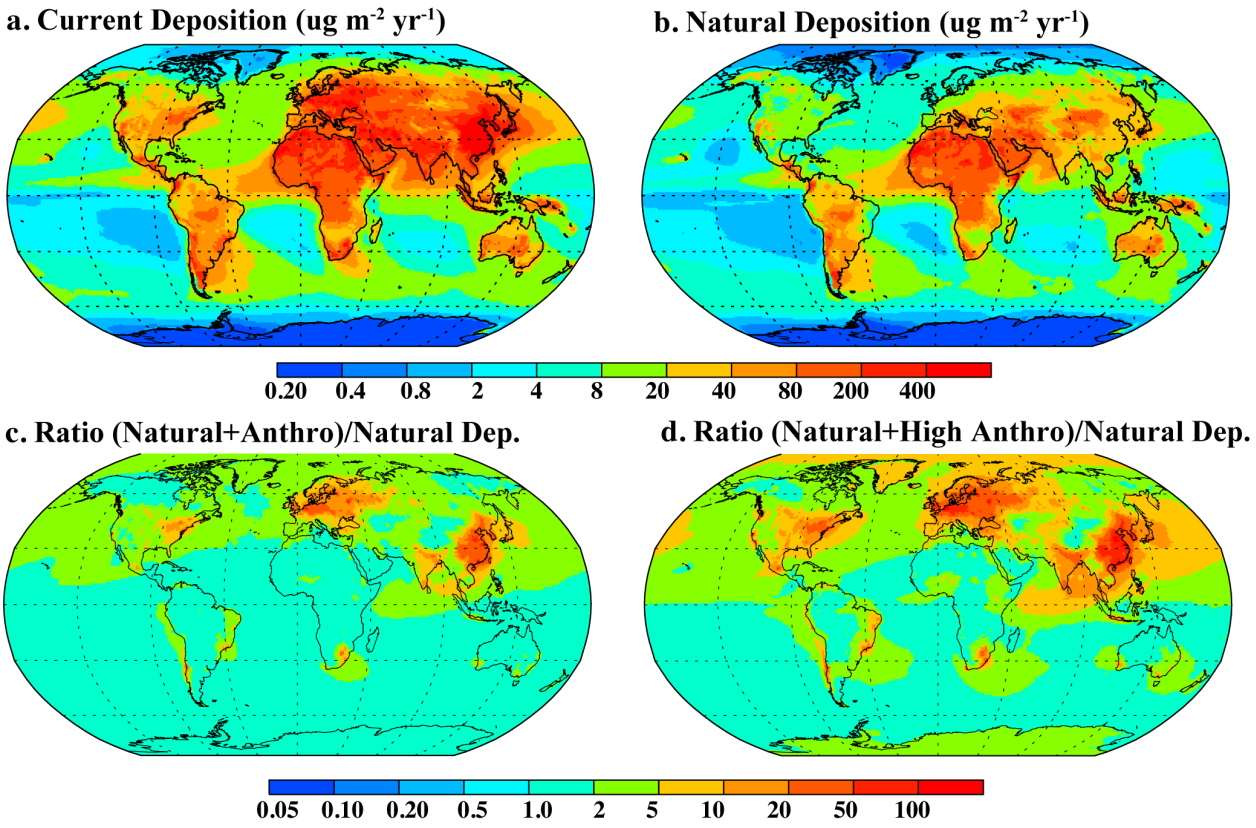

Figure 6. Spatial map of modeled deposition in the Community Atmosphere Model (CAM) (v6) results in the current climate of Mo in PM_{10} aerosols (μg m^{-2} yr^{-1}) for (a) the current (natural and anthropogenic) climate best estimate and (b) with natural sources only. The ratio of natural to total Mo deposition are displayed as (c) the ratio of Mo deposition in the current climate (natural and best estimate anthropogenic) over natural deposition and (d) the ratio of Mo deposition in the current climate with the 'high' anthropogenic estimate case (natural and high anthropogenic) over natural deposition.

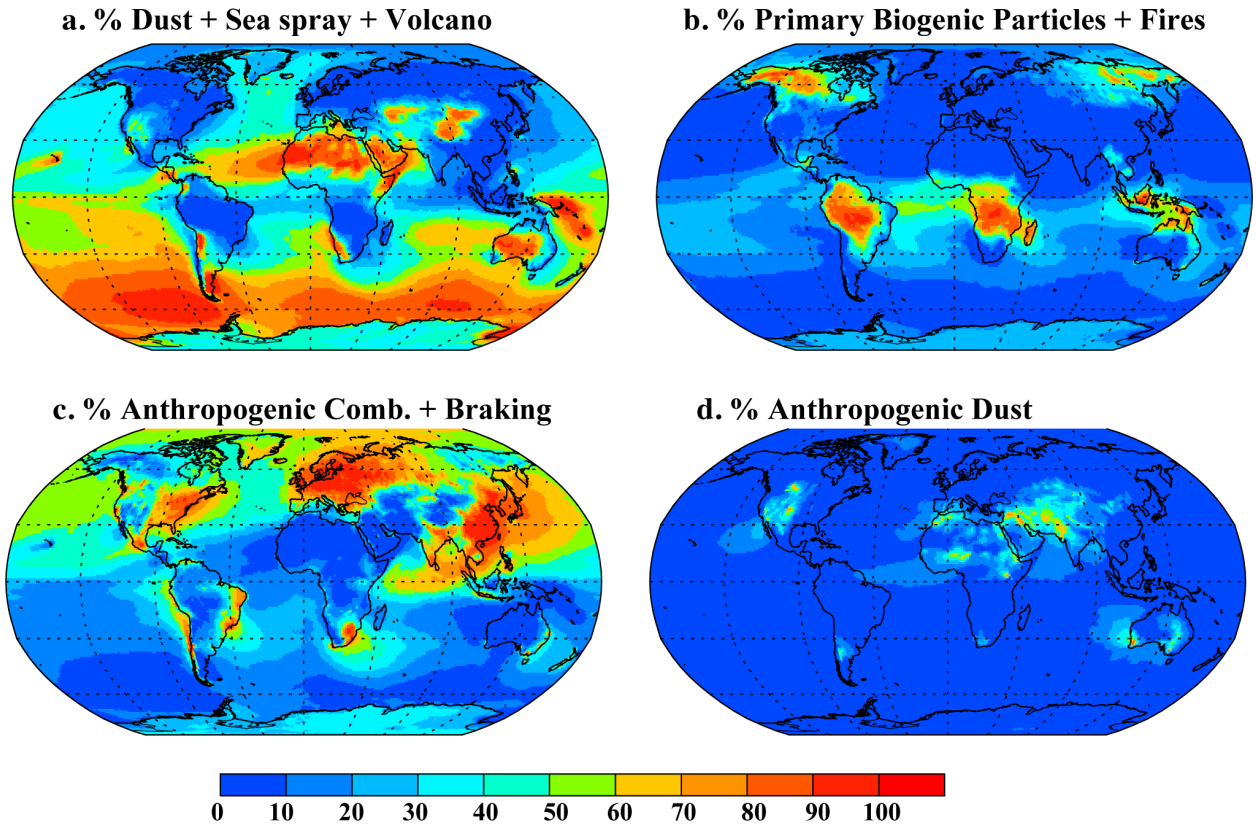

1348

1349 **Figure 7.** Percentage of Mo deposition in the best estimate case in the current climate from
1350 different sources in the Community Atmosphere Model (CAM) (v6): (a) natural desert dust, sea-
1351 spray aerosols, and volcanoes, (b) primary biogenic particles (PBP) and wildfires from natural
1352 ecosystems, (c) anthropogenic combustion and braking emissions, and (d) anthropogenic land
1353 use and agricultural dust.

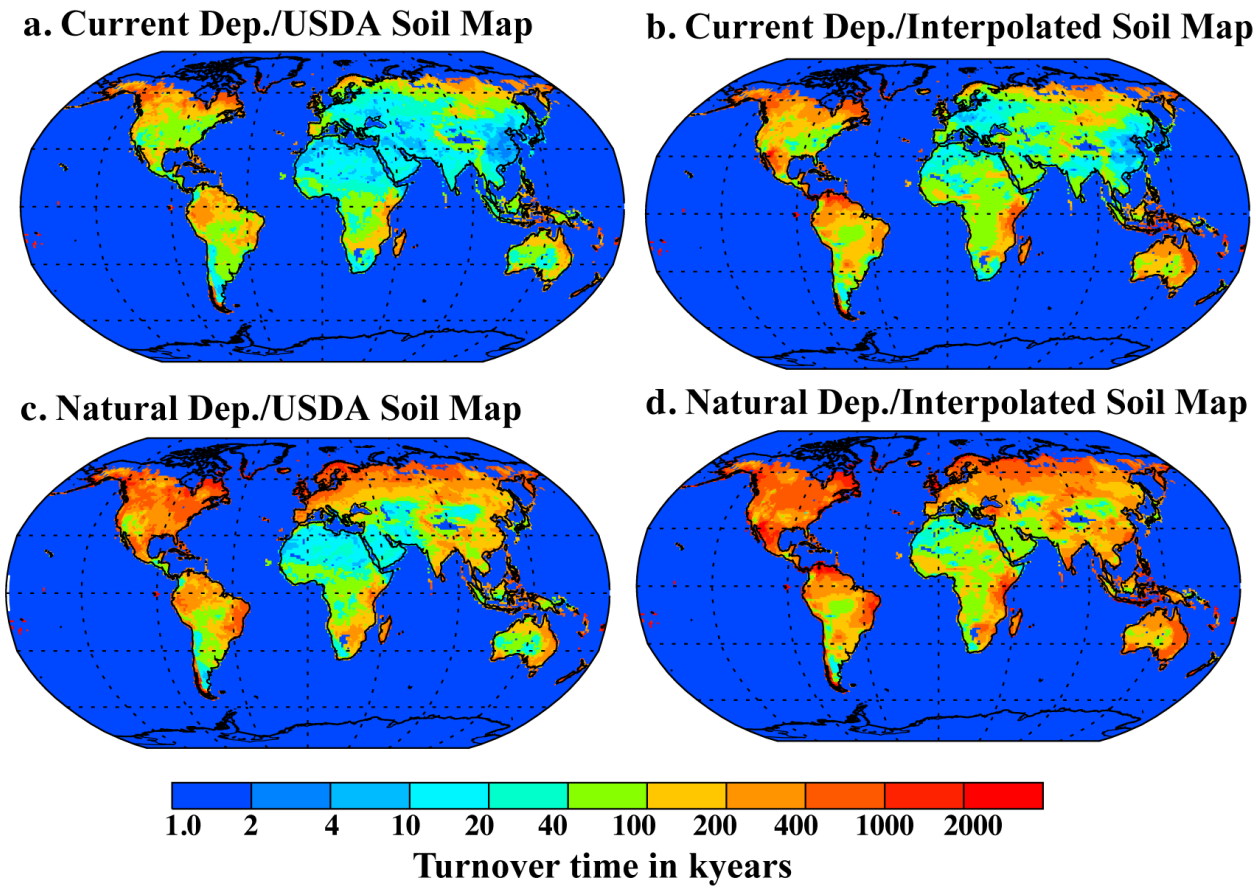

Figure 8. Turnover time (kiloyears) of soil Mo from current (natural plus anthropogenic) deposition in the Community Atmosphere Model (CAM) (v6) in the current climate calculated by (a) the median Mo amounts in USDA soil orders (Supporting Information Table S1; Data Set 3) and (b) and using kriging interpolation, and turnover time of soil Mo from natural deposition only calculated by the median Mo amounts in USDA soil orders (Supporting Information Table S1; Data Set 3) (c) and (d) and using kriging interpolation. Turnover time is estimated as the amount of Mo in the top meter of soil over the deposition flux calculated in the model for the current and natural cases.

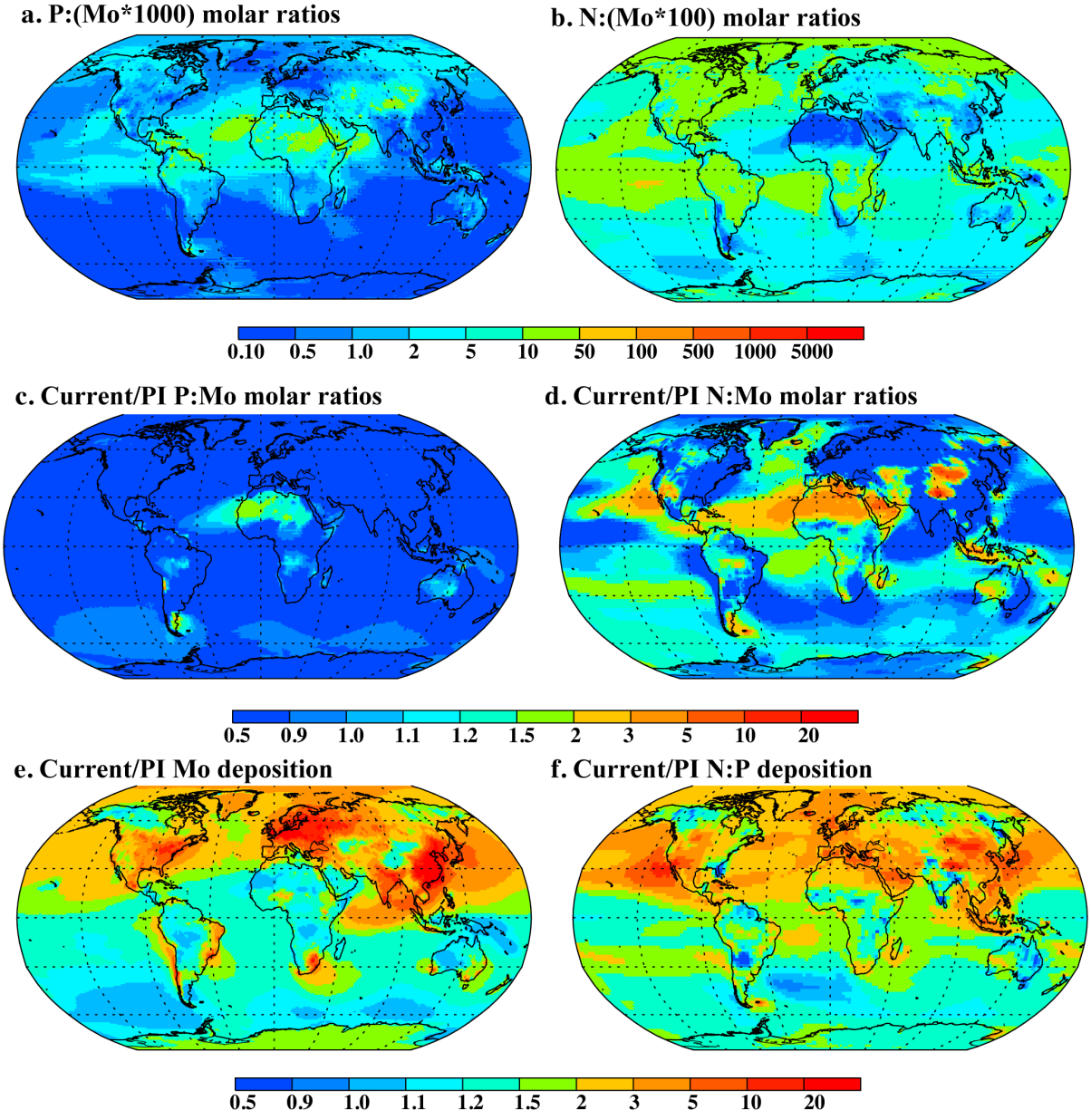

1363

1364 **Figure 9.** Spatial distribution of current (natural plus anthropogenic) modeled atmospheric

1365 deposition of (a) P:(Mo*1000) and (b) N:(Mo*100) molar ratios. (c) Ratios of current to

1366 preindustrial P:Mo, (d) N:No, (e) Mo only, and (f) N:P atmospheric deposition in the

1367 Community Atmosphere Model (CAM) (v6). Current and preindustrial estimates of atmospheric

1368 N and P deposition are derived from the same methodology as described in Brahney et al.,

1369 (2015).

1370 **Table 1.** Concentrations of Mo in sources and atmospheric Mo budgets based on simulations
1371 from the Community Atmosphere Model (CAM) (v6). The numbers in brackets represent the
1372 range of values, while in the parentheses in global source represent the percent (%) of the
1373 aerosols which are in the fine mode ($PM_{2.5}$).

Source	**Mo composition (mg kg^{-1})**	**Composition Citation**	**Global source Mo (Gg yr^{-1}) [ranges] (% fine)**	**Global source Mo (Gg yr^{-1}) (Nraigu, 1989; Nriagu & Pacyna, 1988)**
Natural sources: Dust	1.1 Mo/dust	Wong et al., 2020b	6.8 [3.3-33] (1)	0.12-2.5
Sea-salt aerosols	0.29 Mo/sea-salt aerosol	Wong et al., 2020b	0.75 [0.38-3.8] (3)	0.01-0.43
Volcanoes	400 Mo/S	Nriagu, 1989; Wong et al., 2020b	0.71 [0.35-3.5] (100)	0.04-0.75
Primary Biogenic Particles	1.0 Mo/PBP	Nriagu, 1989	0.49 [0.25-2.5] (10)	0.04-0.75
Wildfires	1000 Mo/BC	Nriagu, 1989	0.02 [0.01-0.1] (81)	0.04-1.1
Anthropogenic sources: Combustion (2010)	5000 Mo/Fe	Rathod et al., in review	11 [11-22] (49)	0.75-5.7
Braking (2010)	500 Mo/PM	Rathod et al., in prep	0.47 [0.47-4.7] (85)	
Agricultural dust	2-5 Mo/agricultural dust	Table S3	2.8 [2.8-7.1] (1)	

1374